

Processes $\gamma\gamma \rightarrow \phi_i\phi_j$ in Inert Higgs Doublet Models and Two Higgs Doublet Models

Khiem Hong Phan^{a,b}, Dzung Tri Tran^{a,b}, Thanh Huy Nguyen^c

^a*Institute of Fundamental and Applied Sciences, Duy Tan University, Ho Chi Minh City 70000, Vietnam*

^b*Faculty of Natural Sciences, Duy Tan University, Da Nang City 50000, Vietnam*

^c*VNUHCM-University of Science, 227 Nguyen Van Cu, District 5, Ho Chi Minh City 70000, Vietnam*

Abstract

In this paper, we present a phenomenological analysis of one-loop induced processes $\gamma\gamma \rightarrow \phi_i\phi_j$, where the CP-even Higgs bosons are denoted as $\phi_{i,j} \equiv h, H$, in high-energy photon-photon collisions, within the frameworks of the Inert Higgs Doublet Model and the Two Higgs Doublet Model. The total cross sections are evaluated as functions of the center-of-mass energy, finding that the cross sections for the considered processes in all the models under investigation are significantly enhanced around the threshold for charged Higgs boson pair production ($\sim 2M_{H^\pm}$). Furthermore, the enhancement factors, defined as the ratios of cross sections of $\gamma\gamma \rightarrow \phi_i\phi_j$ in the investigated models to those for $\gamma\gamma \rightarrow hh$ in the Standard Model, are examined in the relevant regions of the model's parameter space. In the Inert Higgs Doublet Model, the factors are studied in the parameter space of (M_{H^\pm}, μ_2^2) and (M_{H^\pm}, λ_2) . In the Two Higgs Doublet Model, the factors are examined in the planes defined by (M_{H^\pm}, t_β) as well as in the space of the charged Higgs mass M_{H^\pm} and the soft-breaking Z_2 parameter m_{12}^2 . Two scenarios characterized by $c_{\beta-\alpha} > 0$ and $c_{\beta-\alpha} < 0$ are studied in further detail. The factors exhibit distinct behaviors between these two scenarios. As a result, it is possible to discriminate between them at future colliders. The dependence of the cross section for the process $\gamma\gamma \rightarrow hH$ on m_{12}^2 provides a potential probe of the soft Z_2 -breaking scale in the Two Higgs Doublet Model.

Keywords: Higgs phenomenology, one-loop corrections, analytic methods for quantum field theory, dimensional regularization.

1. Introduction

Measuring scalar Higgs self-couplings, including Standard Model-like Higgs trilinear and quadratic couplings, as well as the couplings between scalar Higgses in many beyond-the-Standard-Model (BSM) scenarios, plays a key role in determining the scalar potential. We can subsequently answer the question of the origin of electroweak symmetry breaking (EWSB). In this scheme, Higgs boson pair production and multi-scalar Higgs production should be measured precisely at future colliders. Recently, searches for Higgs boson pair production in final states such as two bottom quarks associated with two photons, four bottom quarks, etc., in proton-proton collisions have been performed at the Large Hadron Collider (LHC), as in [1, 2, 3, 4, 5, 6, 7, 8, 9, 10, 11, 12]. It is well known that measurements of Higgs self-couplings are rather challenging at the LHC. The results from the study in [13, 14] show that the expected accuracy in the measurement of trilinear Higgs self-couplings would be about 20%–30% at the high luminosity of 3000 fb^{-1} . We know that the physics program of future lepton colliders (LC) will be complementary to that

Email address: phanhongkiem@duytan.edu.vn (Khiem Hong Phan)

of the LHC in many aspects, as studied in [15]. Furthermore, the LC can significantly improve LHC measurements in many cases. More importantly, photon-photon collisions are an option at the LC [16, 17], where scalar Higgs pair production ($\phi_i\phi_j$) can be measured via the channels $f\bar{f} \rightarrow f\bar{f}\gamma^*\gamma^* \rightarrow f\bar{f}\phi_i\phi_j$ for $f \equiv e, \mu$. In this regard, the LC could open a window for probing new physics signals through multi-scalar Higgs production.

From a theoretical calculation perspective, one-loop corrections to double Higgs production at the LHC have been calculated in the Standard Model (SM), the Higgs Extensions of the Standard Models (HESM), as well as in other BSM frameworks by many research groups. For example, it is worth mentioning notable works in [18, 19, 20, 21, 22, 23, 24, 25, 26, 27, 28, 29, 30, 31, 32, 33, 34, 35, 36, 37, 38, 39, 40, 41, 42, 43, 44, 45, 46, 47, 48, 49, 50, 51, 52, 53, 54, 55, 56, 57, 58, 59, 60, 61, 62, 63, 64, 65, 66, 67, 68, 69, 70, 71, 72, 73, 74, 75, 76, 77, 78], for further reviews in [79] and the related references therein. Additionally, one-loop corrections for hh production in high-energy $\gamma\gamma$ collisions in the SM, HESM, and other BSM models have been computed in Refs. [80, 81, 82, 83, 84, 85, 86, 87, 88, 89, 90, 91, 92, 93, 94]. Other computations for one-loop corrections to Higgs boson pair production at future linear lepton colliders, including multi-TeV muon colliders, have been performed in Refs. [95, 96, 97, 98] and the additional references therein. Furthermore, double pseudo-scalar Higgs A^0A^0 production at a $\gamma\gamma$ collider in the Two Higgs Doublet Model has been reported in Ref. [99]. One-loop contributions to the process $\gamma\gamma \rightarrow \phi_i\phi_j$ with CP-even Higgses $\phi_{i,j} \equiv h, H$ in high-energy $\gamma\gamma$ collisions, valid for the Higgs Extensions of the Standard Models (HESM), are necessary. In our previous paper, analytic formulas for the concerned processes were reported [100].

In this paper, we present the phenomenological analysis of these processes at high-energy $\gamma\gamma$ collisions in the Inert Higgs Doublet Model (IHDM) and the Two Higgs Doublet Model (THDM). In the phenomenological analysis, cross sections are shown as functions of center-of-mass energies. Furthermore, the enhancement factors, defined as the ratios of cross sections of $\gamma\gamma \rightarrow \phi_i\phi_j$ in the HESMs to the corresponding ones for $\gamma\gamma \rightarrow hh$ in the Standard Model, are examined in the parameter space of the models under consideration. The paper is structured as follows. We briefly review the HESM in the next section. The phenomenological studies for the HESM are discussed in section 3. In section 4, we present the conclusion and outlook of the paper. In appendices A and B, we derive the couplings that appear in the calculations.

2. Higgs Extensions of the Standard Model

Two typical Higgs extensions of the Standard Model are studied in this paper. The first model is the Inert Higgs Doublet Model, which is reviewed in subsection 2.1. We then discuss the Two Higgs Doublet Model in subsection 2.2.

2.1. Inert Higgs Doublet Models

In the IHDM, an inert scalar $SU(2)_L$ doublet is included in the potential of the SM. The inert scalar particles serve as dark matter candidates. For a review of the theory and phenomenological studies of the IHDM in detail, we refer to the following papers [101, 102, 103, 104, 105, 106, 107, 108, 109, 110, 111, 112, 113]. The scalar potential of the IHDM is expressed as follows:

$$\begin{aligned} \mathcal{V}_{\text{IHDM}}(\phi_1, \phi_2) = & \mu_1^2|\phi_1|^2 + \mu_2^2|\phi_2|^2 + \lambda_1|\phi_1|^4 + \lambda_2|\phi_2|^4 + \lambda_3|\phi_1|^2|\phi_2|^2 + \lambda_4|\phi_1^\dagger\phi_2|^2 \\ & + \frac{\lambda_5}{2} \left\{ (\phi_1^\dagger\phi_2)^2 + \text{h.c.} \right\}. \end{aligned} \quad (1)$$

The potential is conserved with respect to the so-called global Z_2 -symmetry, e.g., $\phi_1 \leftrightarrow +\phi_1$, $\phi_2 \leftrightarrow -\phi_2$. In this case, the scalar ϕ_2 is odd, and ϕ_1 and all particles in the SM are even under

the Z_2 -transformation. As mentioned, the Z_2 -symmetry remains unbroken after the EWSB. The field ϕ_2 then has a zero vacuum expectation value (VEV), while the field ϕ_1 develops a non-zero VEV (v). The two scalar fields are then expanded around their VEVs for the EWSB as follows:

$$\phi_1 = \begin{pmatrix} G^\pm \\ \frac{1}{\sqrt{2}}(v + h + iG^0) \end{pmatrix}, \quad (2)$$

$$\phi_2 = \begin{pmatrix} H^\pm \\ \frac{1}{\sqrt{2}}(H + iA^0) \end{pmatrix}. \quad (3)$$

Where the VEV is fixed at $v \sim 246$ GeV (as in the SM case). The Goldstone bosons G^\pm , G^0 give the masses for the W^\pm boson and the Z boson, respectively. There is no mixing between h and H . The physical spectrum of the IHDM after the EWSB consists of three neutral scalar physical states: two CP-even Higgses h , H and a CP-odd Higgs A_0 . Furthermore, we have a pair of singly charged Higgs bosons H^\pm in this model. In the spectrum, the neutral scalar Higgs h is identical to the SM-like Higgs boson discovered at the LHC. The masses of the scalar bosons are calculated from the model parameters as follows:

$$M_h^2 = -2\mu_1^2 = 2\lambda_1 v^2, \quad (4)$$

$$M_H^2 = \mu_2^2 + \frac{v^2}{2}\lambda_L, \quad (5)$$

$$M_{A^0}^2 = \mu_2^2 + \frac{v^2}{2}\lambda_R, \quad (6)$$

$$M_{H^\pm}^2 = \mu_2^2 + \frac{v^2}{2}\lambda_3. \quad (7)$$

We have used $\lambda_{L/R} = \lambda_3 + \lambda_4 \pm \lambda_5$. As mentioned in the previous paragraphs, the global Z_2 -symmetry is unbroken after the EWSB. The "inert" Higgs bosons such as H^\pm , A^0 , and H have an odd number under the Z_2 -transformation. Subsequently, the "inert" Higgs bosons do not couple to the SM particles. Therefore, the lightest neutral scalar bosons may be considered as dark matter candidates.

As a consequence of the unbroken Z_2 -symmetry, the Yukawa Lagrangian of the IHDM must be the same as that of the SM. In detail, the Yukawa Lagrangian is expressed as follows:

$$\mathcal{L}_{\text{Yukawa}}^{\text{IHDM}} = - \sum_{f=u,d,\ell} g_{hff} \cdot h \bar{f} f + \dots, \quad (8)$$

where the Yukawa coupling is given by $g_{hff} = m_f/v$ for fermion f . All the couplings involving the computed processes $\gamma\gamma \rightarrow \phi_i\phi_j$ in the IHDM are listed in Table 1 (for all physical couplings) and Table 2 (for unphysical particles). We emphasize that the processes $\gamma\gamma \rightarrow hH$ are forbidden in the IHDM due to the Z_2 -symmetry. Therefore, we have only $\phi_i\phi_j \equiv hh$, HH in this case. The detailed expressions for all the concerned couplings are derived in appendix A.

| Vertices | Notations | Coupling |
|-------------------------------|--|--|
| $hW_\mu W_\nu$ | $g_{hWW} \cdot g_{\mu\nu}$ | $i \left(\frac{2M_W^2}{v} \right) \cdot g_{\mu\nu}$ |
| $hZ_\mu Z_\nu$ | $g_{hZZ} \cdot g_{\mu\nu}$ | $i \left(\frac{M_Z^2}{v} \right) \cdot g_{\mu\nu}$ |
| $hH^\pm H^\mp$ | $g_{hH^\pm H^\mp}$ | $i \frac{2(\mu_2^2 - M_{H^\pm}^2)}{v}$ |
| $Z_\mu H^\pm(p_1) H^\mp(p_2)$ | $g_{ZH^\pm H^\mp} \cdot (p_1 - p_2)_\mu$ | $i \left(\frac{M_Z c_{2W}}{v} \right) \cdot (p_1 - p_2)_\mu$ |
| $A_\mu H^\pm(p_1) H^\mp(p_2)$ | $g_{AH^\pm H^\mp} \cdot (p_1 - p_2)_\mu$ | $i \left(\frac{M_Z s_{2W}}{v} \right) \cdot (p_1 - p_2)_\mu$ |
| hhh | g_{hhh} | $-i \left(\frac{3M_h^2}{v} \right)$ |
| hHH | g_{hHH} | $i \frac{2(\mu_2^2 - M_H^2)}{v}$ |
| $H(p_2) H^\pm(p_1) W_\mu^\mp$ | $g_{HH^\pm W} \cdot (p_1 - p_2)_\mu$ | $\pm i \left(\frac{M_W}{v} \right) \cdot (p_1 - p_2)_\mu$ |
| $H^\pm H^\mp A_\mu A_\nu$ | $g_{AAH^\pm H^\mp} \cdot g_{\mu\nu}$ | $i \left(\frac{M_Z^2 s_{2W}^2}{v^2} \right) \cdot g_{\mu\nu}$ |
| $HH^\pm W_\nu^\mp A_\mu$ | $g_{HH^\pm W A} \cdot g_{\mu\nu}$ | $i \left(\frac{2M_Z^2 c_W^2 s_W}{v^2} \right) \cdot g_{\mu\nu}$ |
| $hhH^\pm H^\mp$ | $g_{hhH^\pm H^\mp}$ | $i \frac{2(\mu_2^2 - M_{H^\pm}^2)}{v^2}$ |
| $HHH^\pm H^\mp$ | $g_{HHH^\pm H^\mp}$ | $-2i\lambda_2$ |
| $hhW_\mu^\pm W_\nu^\mp$ | $g_{hhWW} \cdot g_{\mu\nu}$ | $i \left(\frac{2M_Z^2 c_W^2}{v^2} \right) \cdot g_{\mu\nu}$ |
| $HHW_\mu^\pm W_\nu^\mp$ | $g_{HHWW} \cdot g_{\mu\nu}$ | $i \left(\frac{2M_Z^2 c_W^2}{v^2} \right) \cdot g_{\mu\nu}$ |

Table 1: We list all couplings (physical couplings) contributing to $\gamma\gamma \rightarrow \phi_i \phi_j$ for the IHDM.

| Vertices | Notations | Coupling |
|-------------------------------|--|--|
| $A_\mu W_\nu^\pm G^\mp$ | $g_{AW^\pm G^\mp} \cdot g_{\mu\nu}$ | $i \left(\frac{2M_Z^2 c_W^2 s_W}{v} \right) \cdot g_{\mu\nu}$ |
| $HH^\pm G^\mp$ | $g_{HH^\pm G^\mp}$ | $i \frac{M_{H^\pm}^2 - M_H^2}{v}$ |
| $hhG^\pm G^\mp$ | $g_{hhG^\pm G^\mp}$ | $-i \left(\frac{M_h^2}{v^2} \right)$ |
| $HHG^\pm G^\mp$ | $g_{HHG^\pm G^\mp}$ | $i \frac{2(\mu_2^2 - M_{H^\pm}^2)}{v^2}$ |
| $A_\mu A_\nu G^\pm G^\mp$ | $g_{AAG^\pm G^\mp} \cdot g_{\mu\nu}$ | $i \left(\frac{M_Z^2 s_{2W}^2}{v^2} \right) \cdot g_{\mu\nu}$ |
| $A_\mu G^\pm(p_1) G^\mp(p_2)$ | $g_{AG^\pm G^\mp} \cdot (p_1 - p_2)_\mu$ | $i \left(\frac{M_Z s_{2W}}{v} \right) \cdot (p_1 - p_2)_\mu$ |

Table 2: We list all vertices (unphysical couplings) in processes $\gamma\gamma \rightarrow \phi_i \phi_j$ in the IHDM.

The parameter space of the IHDM for our analysis is included as follows:

$$\mathcal{P}_{\text{IHDM}} = \{\mu_2^2, \lambda_2^2, M_h^2 \sim 125. \text{GeV}, M_H^2, M_{A^0}^2, M_{H^\pm}^2\}. \quad (9)$$

We are going to review the current constraints on the physical parameter space in the IHDM given in Eq. 9. The constraints for the physical parameter space can be obtained by including the theoretical conditions and the experimental data. In the perspective of the experimental data, we take into account the Electroweak Precision Tests (EWPT) of the IHDM, dark matter search at the LHC, as well as the LEP data. The topics have been studied in Refs. [101, 102, 103, 104]. Additionally, the implications for loop-induced decays of the SM-like Higgs (h) to $V\gamma$ with $V \equiv Z, \gamma$ in the IHDM framework, e.g. the decay process $h \rightarrow \gamma\gamma$, have been reported in [105, 112, 113], and decay channels $h \rightarrow Z\gamma$ have been examined in [112, 113]. Furthermore, searching for signals of the IHDM at future colliders has been performed in Refs. [106, 107, 108, 109, 110, 111]. In the theoretical side, the most important theoretical constraints are obtained from the conditions that the models follow tree-level unitarity, vacuum stability, and the perturbative regime. The theoretical constraints give the limitations on the Higgs self-couplings λ_i for $i = 1, 2, \dots, 5$ and μ_2 . Taking the theoretical and experimental constraints from the above-mentioned papers, one can select the parameter space for the IHDM as follows: we can take $5 \text{ GeV} \leq M_H \leq 150 \text{ GeV}$, $70 \text{ GeV} \leq M_{H^\pm}, M_{A^0} \leq 1000 \text{ GeV}$, $|\mu_2| \leq 500 \text{ GeV}$, and $0 \leq \lambda_2 \leq 8\pi$.

2.2. Two Higgs Doublet Models

We now consider the second kind of Higgs sector extension of the Standard Model, namely the Two Higgs Doublet Models, in this paper. For a comprehensive review of the theory and phenomenological studies of the THDM, we refer the reader to Ref. [114] for further information. The model is briefly summarized in this section. A complex Higgs doublet with hypercharge $Y = 1/2$ is added to the scalar sector of the SM. The scalar potential takes the form:

$$\begin{aligned} \mathcal{V}_{\text{THDM}}(\phi_1, \phi_2) = & m_{11}^2 \phi_1^\dagger \phi_1 + m_{22}^2 \phi_2^\dagger \phi_2 - \left[m_{12}^2 \phi_1^\dagger \phi_2 + \text{h.c.} \right] + \frac{\lambda_1}{2} (\phi_1^\dagger \phi_1)^2 + \frac{\lambda_2}{2} (\phi_2^\dagger \phi_2)^2 \\ & + \lambda_3 (\phi_1^\dagger \phi_1) (\phi_2^\dagger \phi_2) + \lambda_4 (\phi_1^\dagger \phi_2) (\phi_2^\dagger \phi_1) + \frac{1}{2} [\lambda_5 (\phi_1^\dagger \phi_2)^2 + \text{h.c.}] \end{aligned} \quad (10)$$

In the present work, the CP-conserving version of the THDM is examined. Subsequently, the parameters in the above potential are set to be real. Additionally, the scalar potential of the THDM respects a Z_2 symmetry, i.e., $\phi_1 \leftrightarrow \phi_1$ and $\phi_2 \leftrightarrow -\phi_2$, except for the soft-breaking terms such as $m_{12}^2 \phi_1^\dagger \phi_2 + \text{h.c.}$, which are added to the potential. Here, the parameter m_{12}^2 characterizes the soft breaking scale of the Z_2 symmetry.

Two scalar doublets are expanded around their VEVs after electroweak symmetry breaking (EWSB) as

$$\phi_k = \begin{bmatrix} \rho_k^+ \\ (v_k + \eta_k + i\xi_k)/\sqrt{2} \end{bmatrix} \quad \text{for } k = 1, 2. \quad (11)$$

The vacuum expectation value is then fixed at $v = \sqrt{v_1^2 + v_2^2} \sim 246 \text{ GeV}$, in agreement with the SM value. After the EWSB, the physical particles in the THDM consist of two CP-even Higgs bosons, h and H , with one of them, h , being identified as the SM-like Higgs boson discovered at the LHC, a CP-odd Higgs boson (A^0), and a pair of charged Higgs bosons (H^\pm). To obtain the physical masses of the new scalar bosons, we perform the following rotations:

$$\begin{pmatrix} \eta_1 \\ \eta_2 \end{pmatrix} = \begin{pmatrix} c_\alpha & -s_\alpha \\ s_\alpha & c_\alpha \end{pmatrix} \begin{pmatrix} H \\ h \end{pmatrix}, \quad (12)$$

$$\begin{pmatrix} \rho_1^\pm \\ \rho_2^\pm \end{pmatrix} = \begin{pmatrix} c_\beta & -s_\beta \\ s_\beta & c_\beta \end{pmatrix} \begin{pmatrix} G^\pm \\ H^\pm \end{pmatrix}, \quad (13)$$

$$\begin{pmatrix} \xi_1 \\ \xi_2 \end{pmatrix} = \begin{pmatrix} c_\beta & -s_\beta \\ s_\beta & c_\beta \end{pmatrix} \begin{pmatrix} G^0 \\ A^0 \end{pmatrix}. \quad (14)$$

The mixing angle β is defined by $t_\beta \equiv \tan \beta = v_2/v_1$. The physical masses of the Higgs bosons are then expressed in terms of the model parameters as follows:

$$M_{H^\pm}^2 = M^2 - \frac{1}{2}\lambda_{45}v^2, \quad (15)$$

$$M_{A^0}^2 = M^2 - \lambda_5 v^2, \quad (16)$$

$$M_h^2 = M_{11}^2 s_{\beta-\alpha}^2 + M_{22}^2 c_{\beta-\alpha}^2 + M_{12}^2 s_{2(\beta-\alpha)}, \quad (17)$$

$$M_H^2 = M_{11}^2 c_{\beta-\alpha}^2 + M_{22}^2 s_{\beta-\alpha}^2 - M_{12}^2 s_{2(\beta-\alpha)} \quad (18)$$

where the parameter M^2 is used as $M^2 = m_{12}^2/(s_\beta c_\beta)$. The elements M_{ij} for $i, j = 1, 2$ are given by

$$M_{11}^2 = (\lambda_1 c_\beta^4 + \lambda_2 s_\beta^4)v^2 + \frac{v^2}{2} \lambda_{345} s_{2\beta}^2, \quad (19)$$

$$M_{22}^2 = M^2 + \frac{v^2}{4} [\lambda_{12} - 2\lambda_{345}] s_{2\beta}^2, \quad (20)$$

$$M_{12}^2 = M_{21}^2 = -\frac{v^2}{2} [\lambda_1 c_\beta^2 - \lambda_2 s_\beta^2 - \lambda_{345} c_{2\beta}] s_{2\beta}. \quad (21)$$

Here, the shorten notation have used as $\lambda_{ij\dots} = \lambda_i + \lambda_j + \dots$.

We present the relevant couplings involved in the amplitude computations for the processes $\gamma\gamma \rightarrow \phi_i \phi_j$ in Tables 3, 4 (for physical couplings) and in Table 5 (for unphysical couplings). These couplings are derived in Appendix B.

| Vertices | Notations | Couplings |
|------------------------------|--|---|
| $hW_\mu W_\nu$ | $g_{hWW} \cdot g_{\mu\nu}$ | $i \left(\frac{2M_W^2}{v} s_{\beta-\alpha} \right) \cdot g_{\mu\nu}$ |
| $HW_\mu W_\nu$ | $g_{HWW} \cdot g_{\mu\nu}$ | $i \left(\frac{2M_W^2}{v} c_{\beta-\alpha} \right) \cdot g_{\mu\nu}$ |
| $hZ_\mu Z_\nu$ | $g_{hZZ} \cdot g_{\mu\nu}$ | $i \left(\frac{2M_Z^2}{v} s_{\beta-\alpha} \right) \cdot g_{\mu\nu}$ |
| $HZ_\mu Z_\nu$ | $g_{HZZ} \cdot g_{\mu\nu}$ | $i \left(\frac{2M_Z^2}{v} c_{\beta-\alpha} \right) \cdot g_{\mu\nu}$ |
| $hH^\pm H^\mp$ | $g_{hH^\pm H^\mp}$ | $i \left[\frac{c_{\alpha+\beta}(4M^2 - 3M_h^2 - 2M_{H^\pm}^2)}{2vs_{2\beta}} + \frac{(2M_{H^\pm}^2 - M_h^2)c_{(\alpha-3\beta)}}{2vs_{2\beta}} \right]$ |
| $Z_\mu H^\pm(p_1)H^\mp(p_2)$ | $g_{ZH^\pm H^\mp} \cdot (p_1 - p_2)_\mu$ | $i \left(\frac{M_Z c_{2W}}{v} \right) \cdot (p_1 - p_2)_\mu$ |
| $A_\mu H^\pm(p_1)H^\mp(p_2)$ | $g_{AH^\pm H^\mp} \cdot (p_1 - p_2)_\mu$ | $i \left(\frac{M_Z s_{2W}}{v} \right) \cdot (p_1 - p_2)_\mu$ |
| hhh | g_{hhh} | $i \frac{3e}{4M_W s_W s_{2\beta}} \left[M^2 c_{\alpha-3\beta} + (M^2 - M_h^2) c_{3\alpha-\beta} + (2M^2 - 3M_h^2) c_{\alpha+\beta} \right]$ |
| HHH | g_{HHH} | $i \frac{3e}{4M_W s_W s_{2\beta}} \left[M^2 s_{\alpha-3\beta} + (M_H^2 - M^2) s_{3\alpha-\beta} + (2M^2 - 3M_H^2) s_{\alpha+\beta} \right]$ |
| hHH | g_{hHH} | $i \frac{[s_{2\alpha}(3M^2 - M_h^2 - 2M_H^2) + M^2 s_{2\beta}]}{v s_{2\beta}} s_{\alpha-\beta}$ |
| Hhh | g_{Hhh} | $i \frac{[s_{2\alpha}(3M^2 - M_H^2 - 2m_h^2) - M^2 s_{2\beta}]}{2vs_{2\beta}} c_{\alpha-\beta}$ |

Table 3: The physical couplings contributing to the considered processes $\gamma\gamma \rightarrow \phi_i \phi_j$ in the THDM.

| Vertices | Notations | Couplings |
|-----------------------------|---------------------------------------|---|
| $HH^\pm H^\mp$ | $g_{HH^\pm H^\mp}$ | $i \left[\frac{s_{\alpha+\beta}(4M^2 - 3M_H^2 - 2M_{H^\pm}^2)}{2v s_{2\beta}} + \frac{(2M_{H^\pm}^2 - M_H^2)s_{\alpha-3\beta}}{2v s_{2\beta}} \right]$ |
| $H(p_1)H^\pm(p_2)W_\mu^\mp$ | $g_{HH^\pm W} \cdot (p_1 - p_2)_\mu$ | $\pm i \left(\frac{M_W}{v} s_{\beta-\alpha} \right) \cdot (p_1 - p_2)_\mu$ |
| $h(p_1)H^\pm(p_2)W_\mu^\mp$ | $g_{hH^\pm W} \cdot (p_1 - p_2)_\mu$ | $\mp i \left(\frac{M_W}{v} c_{\alpha-\beta} \right) \cdot (p_1 - p_2)_\mu$ |
| $H^\pm H^\mp A_\mu A_\nu$ | $g_{H^\pm H^\mp AA} \cdot g_{\mu\nu}$ | $i \left(\frac{4M_W^2 s_W^2}{v^2} \right) \cdot g_{\mu\nu}$ |
| $HH^\pm W_\mu^\mp A_\nu$ | $g_{HH^\pm WA} \cdot g_{\mu\nu}$ | $i \left(\frac{2M_W^2 s_W}{v^2} s_{\alpha-\beta} \right) \cdot g_{\mu\nu}$ |
| $hH^\pm W_\mu^\mp A_\nu$ | $g_{hH^\pm WA} \cdot g_{\mu\nu}$ | $i \left(\frac{2M_W^2 s_W}{v^2} c_{\alpha-\beta} \right) \cdot g_{\mu\nu}$ |
| $hHH^\pm H^\mp$ | $g_{HhH^\pm H^\mp}$ | $i\lambda_{HhH^\pm H^\mp}$ [in Eq. (38)] |
| $HHH^\pm H^\mp$ | $g_{HHH^\pm H^\mp}$ | $i\lambda_{HHH^\pm H^\mp}$ [in Eq. (42)] |
| $hhH^\pm H^\mp$ | $g_{hhH^\pm H^\mp}$ | $i\lambda_{hhH^\pm H^\mp}$ [in Eq. (43)] |
| $hhW_\mu^\pm W_\nu^\mp$ | $g_{hhWW} \cdot g_{\mu\nu}$ | $i \left(\frac{4M_W^2}{v^2} \right) \cdot g_{\mu\nu}$ |
| $HHW_\mu^\pm W_\nu^\mp$ | $g_{HHWW} \cdot g_{\mu\nu}$ | $i \left(\frac{4M_W^2}{v^2} \right) \cdot g_{\mu\nu}$ |

Table 4: Additional, the physical couplings contributing to the considered processes $\gamma\gamma \rightarrow \phi_i \phi_j$ in the THDM.

| Vertices | Notations | Couplings |
|------------------------------|--|--|
| $A_\mu W_\nu^\pm G^\mp$ | $g_{AW^\pm G^\mp} \cdot g_{\mu\nu}$ | $i \left(\frac{2M_W^2 s_W}{v} \right) \cdot g_{\mu\nu}$ |
| $HH^\pm G^\mp$ | $g_{HH^\pm G^\mp}$ | $i \left(\frac{e}{2M_W s_W} s_{\alpha-\beta} \right) (M_{H^\pm}^2 - M_H^2)$ |
| $A_\mu A_\nu G^\pm G^\mp$ | $g_{AAG^\pm G^\mp} \cdot g_{\mu\nu}$ | $i \left(\frac{4M_W^2 s_W^2}{v^2} \right) \cdot g_{\mu\nu}$ |
| $A_\mu G^\pm(p_1)G^\mp(p_2)$ | $g_{AG^\pm G^\mp} \cdot (p_1 - p_2)_\mu$ | $i \left(\frac{2M_W s_W}{v} \right) \cdot (p_1 - p_2)_\mu$ |
| $hHG^\pm G^\mp$ | $g_{hHG^\pm G^\mp}$ | $i\lambda_{hHG^\pm G^\mp}$ [in Eq. (39)] |
| $hhG^\pm G^\mp$ | $g_{hhG^\pm G^\mp}$ | $i\lambda_{hhG^\pm G^\mp}$ [in Eq. (44)] |
| $HHG^\pm G^\mp$ | $g_{HHG^\pm G^\mp}$ | $i\lambda_{HHG^\pm G^\mp}$ [in Eq. (45)] |

Table 5: Unphysical couplings involving to the processes under investigations are shown.

Finally, we pay attention to the Yukawa sector in the THDM. In order to avoid Tree-level Flavor-Changing Neutral Currents (FCNCs), the discrete Z_2 -symmetry may be proposed in the THDM as in [115]. The Z_2 -parity assignments for all fermions and the definition for four types

of the THDM based on the couple of the scalar with fermions are shown in [125]. The Yukawa Lagrangian is then written in the mass eigenstates as in [114]

$$\mathcal{L}_{\text{Yukawa}} = - \sum_{f=u,d,\ell} (g_{hff} \cdot \bar{f} f h + g_{Hff} \cdot \bar{f} f H - i g_{A^0 ff} \cdot \bar{f} \gamma_5 f A^0) + \dots, \quad (22)$$

We show the Yukawa couplings of CP-even with fermions for four types of the THDM in Table 6, see [114, 126] for further detail.

| Type | g_{huu} | g_{hdd} | $g_{h\ell\ell}$ | g_{Huu} | g_{Hdd} | $g_{H\ell\ell}$ |
|------|--|---|--|--|---|--|
| I | $\frac{m_u}{\sqrt{2}v} \frac{c_\alpha}{s_\beta}$ | $\frac{m_d}{\sqrt{2}v} \frac{c_\alpha}{s_\beta}$ | $\frac{m_\ell}{\sqrt{2}v} \frac{c_\alpha}{s_\beta}$ | $\frac{m_u}{\sqrt{2}v} \frac{s_\alpha}{s_\beta}$ | $\frac{m_d}{\sqrt{2}v} \frac{s_\alpha}{s_\beta}$ | $\frac{m_\ell}{\sqrt{2}v} \frac{s_\alpha}{s_\beta}$ |
| II | $\frac{m_u}{\sqrt{2}v} \frac{c_\alpha}{s_\beta}$ | $-\frac{m_d}{\sqrt{2}v} \frac{s_\alpha}{c_\beta}$ | $-\frac{m_\ell}{\sqrt{2}v} \frac{s_\alpha}{c_\beta}$ | $\frac{m_u}{\sqrt{2}v} \frac{s_\alpha}{s_\beta}$ | $-\frac{m_d}{\sqrt{2}v} \frac{c_\alpha}{c_\beta}$ | $-\frac{m_\ell}{\sqrt{2}v} \frac{c_\alpha}{c_\beta}$ |
| X | $\frac{m_u}{\sqrt{2}v} \frac{c_\alpha}{s_\beta}$ | $\frac{m_d}{\sqrt{2}v} \frac{c_\alpha}{s_\beta}$ | $-\frac{m_\ell}{\sqrt{2}v} \frac{s_\alpha}{c_\beta}$ | $\frac{m_u}{\sqrt{2}v} \frac{s_\alpha}{s_\beta}$ | $\frac{m_d}{\sqrt{2}v} \frac{s_\alpha}{s_\beta}$ | $-\frac{m_\ell}{\sqrt{2}v} \frac{c_\alpha}{c_\beta}$ |
| Y | $\frac{m_u}{\sqrt{2}v} \frac{c_\alpha}{s_\beta}$ | $-\frac{m_d}{\sqrt{2}v} \frac{s_\alpha}{c_\beta}$ | $\frac{m_\ell}{\sqrt{2}v} \frac{c_\alpha}{s_\beta}$ | $\frac{m_u}{\sqrt{2}v} \frac{s_\alpha}{s_\beta}$ | $-\frac{m_d}{\sqrt{2}v} \frac{c_\alpha}{c_\beta}$ | $\frac{m_\ell}{\sqrt{2}v} \frac{s_\alpha}{s_\beta}$ |

Table 6: We show all the Yukawa couplings of CP-even Higgses to fermions for all types of THDMs.

The parameter space $\mathcal{P}_{\text{THDM}}$ for THDM is include as follows

$$\mathcal{P}_{\text{THDM}} = \{M_h^2 \sim 125.\text{GeV}, M_H^2, M_{A^0}^2, M_{H^\pm}^2, m_{12}^2, t_\beta, s_{\beta-\alpha}\}. \quad (23)$$

As in the case of the IHDM, we first summarize the current constraints on the parameter space of the THDM, given in Eq. 23. Both theoretical conditions and experimental data are taken into account, from which the allowed regions of the parameter space of the THDM are determined. Theoretical constraints arise from the requirements that the model remains within the perturbative regime, satisfies tree-level unitarity, and ensures vacuum stability of the scalar potential. These topics have been discussed in detail in Refs. [116, 117, 118, 119, 121] and references therein. We also consider electroweak precision tests (EWPT) in the context of the THDM, based on experimental data. Relevant implications for these constraints from LEP are reported in Refs. [122, 123]. The allowed mass ranges of the scalar particles in the THDM have been investigated at LEP, the Tevatron, and the LHC, as reviewed in Ref. [120]. Furthermore, one-loop induced decays of the SM-like Higgs boson, such as $h \rightarrow \gamma\gamma$ and $h \rightarrow Z\gamma$, have also been analyzed within the THDM in Refs. [112, 113] and references therein. By combining all of the above constraints, the physical parameter ranges can be chosen as follows: $126 \text{ GeV} \leq M_H \leq 1000 \text{ GeV}$, $60 \text{ GeV} \leq M_{A^0} \leq 1000 \text{ GeV}$, and $80 \text{ GeV} \leq M_{H^\pm} \leq 1000 \text{ GeV}$ for Type-I and Type-X THDMs. For Type-II and Type-Y, the physical parameters are scanned in the ranges: $500 \text{ GeV} \leq M_H \leq 1000 \text{ GeV}$, $500 \text{ GeV} \leq M_{A^0} \leq 1000 \text{ GeV}$, and $580 \text{ GeV} \leq M_{H^\pm} \leq 1500 \text{ GeV}$. The soft Z_2 -breaking parameter is chosen as $m_{12}^2 = M_H^2 s_\beta c_\beta$. Finally, additional constraints in the (t_β, M_{H^\pm}) plane are examined by incorporating flavor physics data, as shown in Ref. [124]. The results in Ref. [124] indicate that small values of t_β are favored to be consistent with flavor experimental constraints. In our complementary analysis, we also explore the phenomenology associated with low t_β scenarios.

3. Phenomenological results

The detailed calculations for $\gamma\gamma \rightarrow \phi_i\phi_j$ with CP-even Higgses $\phi_{i,j} \equiv h, H$ in the HESM have been reported in our previous work [100]. In this paper, we focus on the phenomenological analysis of the concerned processes in the IHDM and the THDM. We are interested in examining the enhancement factors $\mu_{\phi_i\phi_j}^{\text{NP}}$ with NP standing for the THDM and the IHDM, respectively, defined as the ratio of the cross-sections of $\gamma\gamma \rightarrow \phi_i\phi_j$ in the HESM to the corresponding ones for $\gamma\gamma \rightarrow hh$ in the SM. The factors are given explicitly by

$$\mu_{\phi_i\phi_j}^{\text{NP}} = \frac{\hat{\sigma}_{\gamma\gamma \rightarrow \phi_i\phi_j}^{\text{NP}}}{\hat{\sigma}_{\gamma\gamma \rightarrow hh}^{\text{SM}}}(\mathcal{P}_{\text{NP}}). \quad (24)$$

In this work, the enhancement factors are examined within the parameter space of the THDM and the IHDM. For the phenomenological results, all physical input parameters in the SM are taken to be the same as those in [125, 126].

3.1. IHDM

Phenomenological studies for the processes $\gamma\gamma \rightarrow \phi_i\phi_j$ in the IHDM are presented in this subsection. In the IHDM, the process $\gamma\gamma \rightarrow hH$ is forbidden by the Z_2 -symmetry. For this reason, we only focus on physical results for the processes $\gamma\gamma \rightarrow hh, HH$ in the IHDM. We note that all physical results in the IHDM presented in the following subsections can be considered as the first outcomes from this work.

3.1.1. Production cross-sections

In Fig. 1, we show cross-sections for $\gamma\gamma \rightarrow hh, HH$ in the IHDM, together with those for hh production in the SM, as functions of center-of-mass energy (CoM, or $\sqrt{\hat{s}_{\gamma\gamma}}$). For the generated data, we select the following parameter space in the IHDM: $M_{H^\pm} = 200$ GeV, $M_H = 150$ GeV, and fix $\lambda_2 = 0.8$ for all cases. We vary $350 \text{ GeV} \leq \sqrt{\hat{s}_{\gamma\gamma}} \leq 1500$ GeV in the plots. Cross-sections are presented for $\mu_2^2 = 0 \text{ GeV}^2$ on the left panel and for 200^2 GeV^2 on the right panel, respectively. In the plots, the black line represents the cross-sections for $\gamma\gamma \rightarrow hh$ in the SM, and the blue (green) line represents the cross-sections for $\gamma\gamma \rightarrow hh, (HH)$ in the IHDM, respectively.

We first comment on the results in the case of $\mu_2^2 = 0 \text{ GeV}^2$. The cross-sections for hh, HH in the IHDM have peaks at $\sqrt{\hat{s}_{\gamma\gamma}} \sim 2M_{H^\pm} = 400$ GeV. In the regions $\sqrt{\hat{s}_{\gamma\gamma}} \leq 750$ GeV, $\hat{\sigma}_{hh,HH}$ in the IHDM are larger than $\hat{\sigma}_{hh}$ in the SM. Beyond the regions of $\sqrt{\hat{s}_{\gamma\gamma}} \geq 750$ GeV, the cross-sections for HH in the IHDM are suppressed in comparison with hh production in both the SM and the IHDM. It is interesting to find that the production cross-sections for $\gamma\gamma \rightarrow hh, HH$ in the IHDM are dominant around the peaks compared with $\hat{\sigma}_{hh}$ in the SM. This indicates that the contributions from singly charged Higgs in the loop of $\gamma\gamma \rightarrow hh, HH$ are significant in these regions.

In the case of $\mu_2^2 = 200^2 \text{ GeV}^2$, we only observe a peak of $\hat{\sigma}_{HH}$ in the IHDM around $\sqrt{\hat{s}_{\gamma\gamma}} \sim 2M_{H^\pm} = 400$ GeV. Furthermore, the data shows that the cross-sections for HH production are dominant in the regions $\sqrt{\hat{s}_{\gamma\gamma}} \leq 750$ GeV, in contrast with the corresponding ones for hh production in both the SM and the IHDM. Beyond the regions $\sqrt{\hat{s}_{\gamma\gamma}} \geq 750$ GeV, $\hat{\sigma}_{HH}$ is suppressed. It is observed that the cross-sections for hh production in the IHDM are smaller than $\hat{\sigma}_{hh}$ in the SM when $\sqrt{\hat{s}_{\gamma\gamma}} \leq 550$ GeV. In the regions of $\sqrt{\hat{s}_{\gamma\gamma}} \geq 550$ GeV, $\hat{\sigma}_{hh}$ in the IHDM tends to the cross-sections for hh production in the SM. This can be explained as follows. Since the hh production in the IHDM are different from those in the SM by the contributions of charged Higgs in the loop of triangle h^* -pole and box diagrams. These contributions depend on M_{H^\pm} and the vertices $hH^\pm H^\mp, hhH^\pm H^\mp$, expressed in terms of μ_2^2 . At large values of μ_2^2 ,

these contributions may be cancelled out. As a result, cross-sections for hh production in the IHDM tend to the corresponding ones in the SM. In another case of HH production, we have no couplings of $HH^\pm H^\mp$ due to the Z_2 -symmetry and the vertex $HHH^\pm H^\mp$ depends on λ_2 . Therefore, we have no such cancellations as mentioned. It is reasonable that the cross-sections for HH production in the IHDM are dominant in the regions $\sqrt{\hat{s}_{\gamma\gamma}} \leq 550$ GeV and they also have a peak at $\sqrt{\hat{s}_{\gamma\gamma}} \sim 2M_{H^\pm} = 400$ GeV.

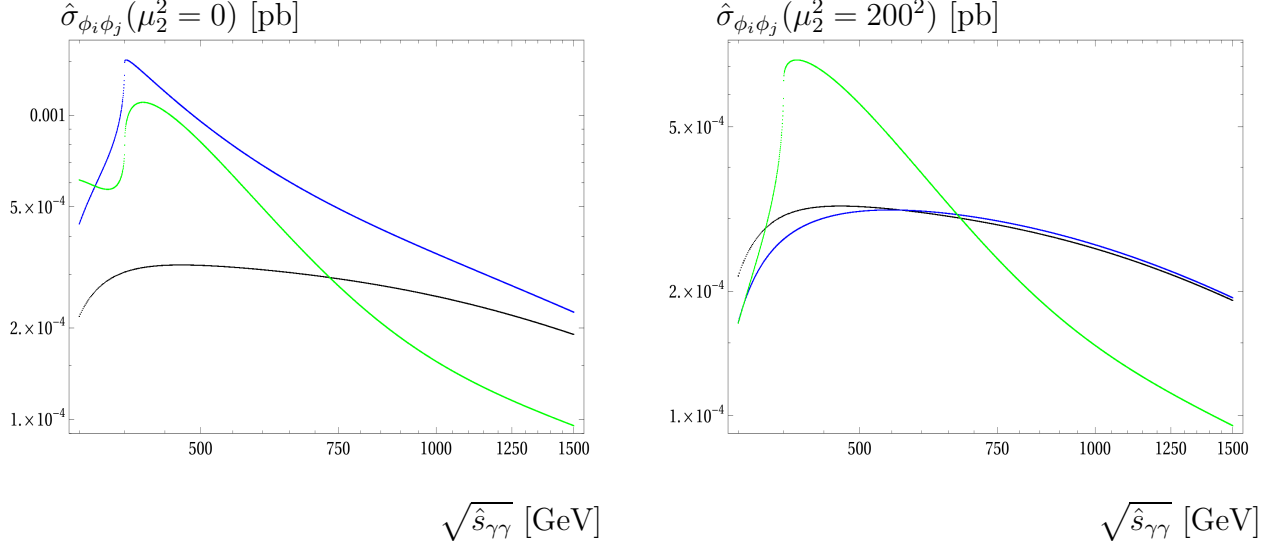


Figure 1: Total cross-sections for $\gamma\gamma \rightarrow hh, HH$ in the SM and IHDM are presented as functions of $\sqrt{\hat{s}_{\gamma\gamma}}$. For the generated data, we select $M_{H^\pm} = 200$ GeV, $M_H = 150$ GeV in this case. We vary $350 \text{ GeV} \leq \sqrt{\hat{s}_{\gamma\gamma}} \leq 1500$ GeV. In the plots below, we fix $\mu_2^2 = 0, 200^2 \text{ GeV}^2$ and $\lambda_2 = 0.8$ for all cases. In the plots, the black line shows $\hat{\sigma}_{hh}$ in the SM. Additionally, the blue (green) line presents $\gamma\gamma \rightarrow hh$ (HH) in the THDM.

3.1.2. Enhancement factors

The enhancement factors given in Eq. 24 are examined in the IHDM. In Fig. 2, the factors for $\gamma\gamma \rightarrow hh, HH$ are scanned in the parameter space of M_{H^\pm}, μ_2^2 . In the following scatter plots, singly charged Higgs masses are varied from $70 \text{ GeV} \leq M_{H^\pm} \leq 600$ GeV and $-200 \text{ GeV} \leq \mu_2 \leq 200$ GeV. Furthermore, we fix $\lambda_2 = 0.8$ and $M_H = 150$ GeV for all cases. The data are generated at $\sqrt{\hat{s}_{\gamma\gamma}} = 500$ (all left panel scatter-plots) GeV and at $\sqrt{\hat{s}_{\gamma\gamma}} = 1000$ GeV (all right panel scatter-plots).

The factors for hh production in the IHDM are first analyzed. Since the cross-sections for hh production are enhanced around the peaks at $\sqrt{\hat{s}_{\gamma\gamma}} \sim 2M_{H^\pm}$, it is not surprising to find that μ_{hh}^{IHDM} becomes largest at $\sqrt{\hat{s}_{\gamma\gamma}} \sim 2M_{H^\pm} = 250$ GeV (for the left plots) and at $\sqrt{\hat{s}_{\gamma\gamma}} \sim 2M_{H^\pm} = 500$ GeV (for the right plots). Around these peaks, the data indicate that the enhancement factors tend to about ~ 1.5 in the limit of $\mu_2^2 \rightarrow M_{H^\pm}^2$, since the contributions of the charged Higgs in the loop are small when $\mu_2^2 \rightarrow M_{H^\pm}^2$ (due to the fact that the couplings of $hH^\pm H^\mp$ and $hhH^\pm H^\mp$ tend to zero in this limit). It is found that the enhancement factors can reach a factor of 6 (for 500 GeV of CoM) and a factor of 13 (for 1000 GeV of CoM) around the peaks. Beyond the peaks, we observe that $1 \leq \mu_{hh}^{\text{IHDM}} \leq 2$.

For the enhancement factors of HH production in the IHDM, we also find that μ_{HH}^{IHDM} becomes largest at $\sqrt{\hat{s}_{\gamma\gamma}} \sim 2M_{H^\pm} = 250$ GeV (for the left plots) and at $\sqrt{\hat{s}_{\gamma\gamma}} \sim 2M_{H^\pm} = 500$ GeV (for the right plots). It is important to realize that μ_{HH}^{IHDM} has different behavior in comparison with

μ_{hh}^{IHDM} . At 500 GeV of CoM, the factors rise to the peak and then decrease rapidly beyond the peak. However, they grow with the charged Higgs masses in the above regions of $M_{H^\pm} \geq \sim 300$ GeV. Because there are no couplings of $HH^\pm H^\mp$ due to the Z_2 -symmetry and the vertex $HHH^\pm H^\mp$ only depends on λ_2 , the factors μ_{HH}^{IHDM} increase with M_{H^\pm} in the high regions of charged Higgs masses.

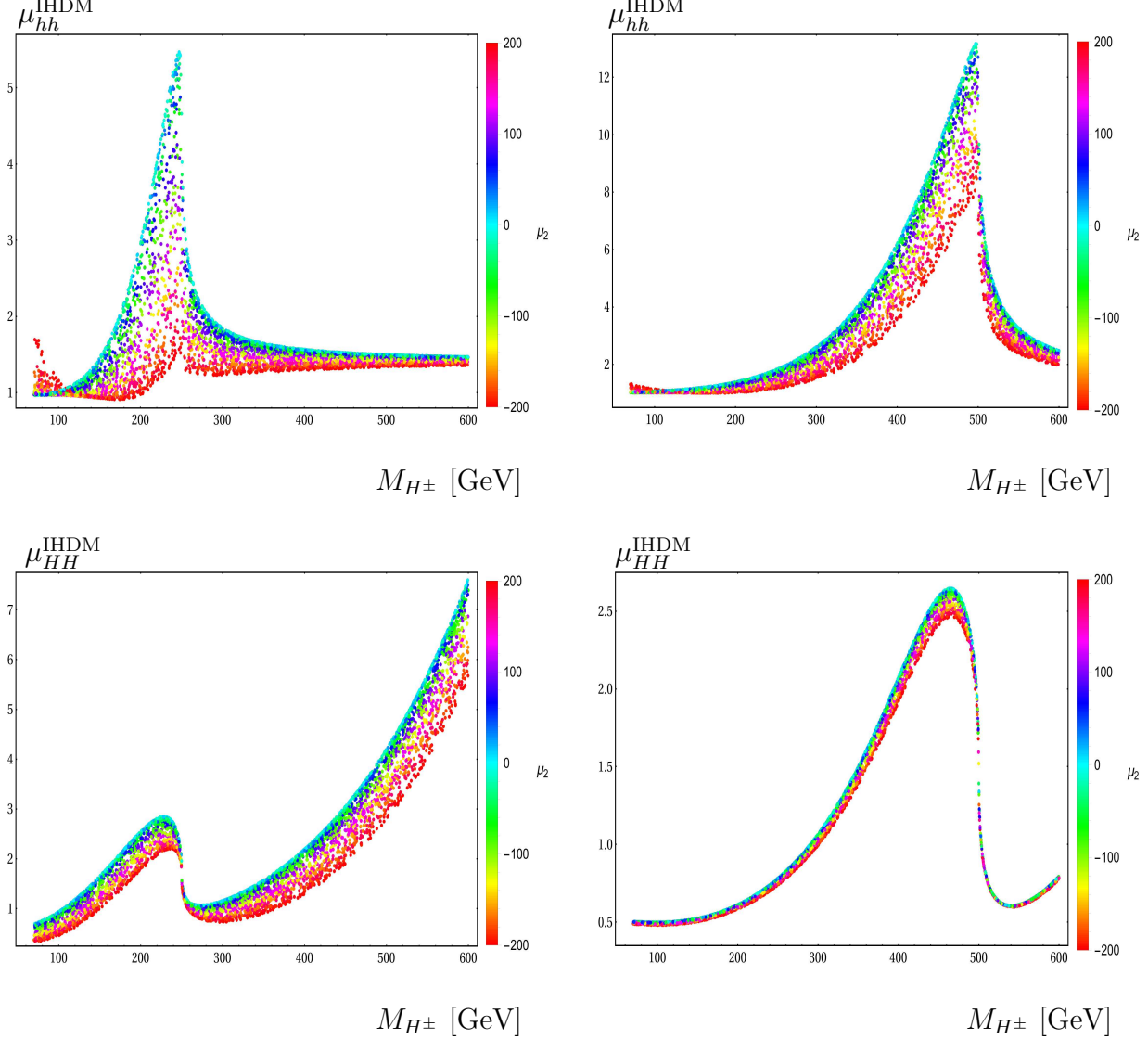


Figure 2: The enhancement factors are presented in the parameter space of M_{H^\pm} , μ_2^2 . Charged Higgs masses are varied as $70 \text{ GeV} \leq M_{H^\pm} \leq 1000 \text{ GeV}$ and $-200 \text{ GeV} \leq \mu_2 \leq 200 \text{ GeV}$. We fix $\lambda_2 = 0.8$ and $M_H = 150 \text{ GeV}$ for all cases. In the plots, we set $\sqrt{\hat{s}_{\gamma\gamma}} = 500 \text{ GeV}$ (for the left panel-plots) and $\sqrt{\hat{s}_{\gamma\gamma}} = 1000 \text{ GeV}$ (for the right panel-plots).

In Fig. 3, the enhancement factors for $\gamma\gamma \rightarrow hh$, HH are generated in the space of M_{H^\pm} , λ_2 . The charged Higgs masses are varied as $70 \text{ GeV} \leq M_{H^\pm} \leq 600 \text{ GeV}$ and $0 \leq \lambda_2 \leq 4$. We fix $\mu_2^2 = 200^2 \text{ GeV}^2$ and $M_H = 150 \text{ GeV}$ for all cases. In the scatter plots, we set $\sqrt{\hat{s}_{\gamma\gamma}} = 500$ (for all left panel plots) GeV and $\sqrt{\hat{s}_{\gamma\gamma}} = 1000 \text{ GeV}$ (for all right panel plots). For the factors μ_{hh}^{IHDM} (as shown in all the above scatter plots), both the couplings $hH^\pm H^\mp$ and $hhH^\pm H^\mp$ are independent of λ_2 . As a result, the factors only depend on M_{H^\pm} . For the factors μ_{HH}^{IHDM} (as shown in all the below scatter plots), it is found that the quadratic-coupling $HHH^\pm H^\mp$ depends

on λ_2 . As a result, the factors depend strongly on λ_2 and M_{H^\pm} . These massive contributions are mainly from the charged Higgs exchanging in the box diagrams.

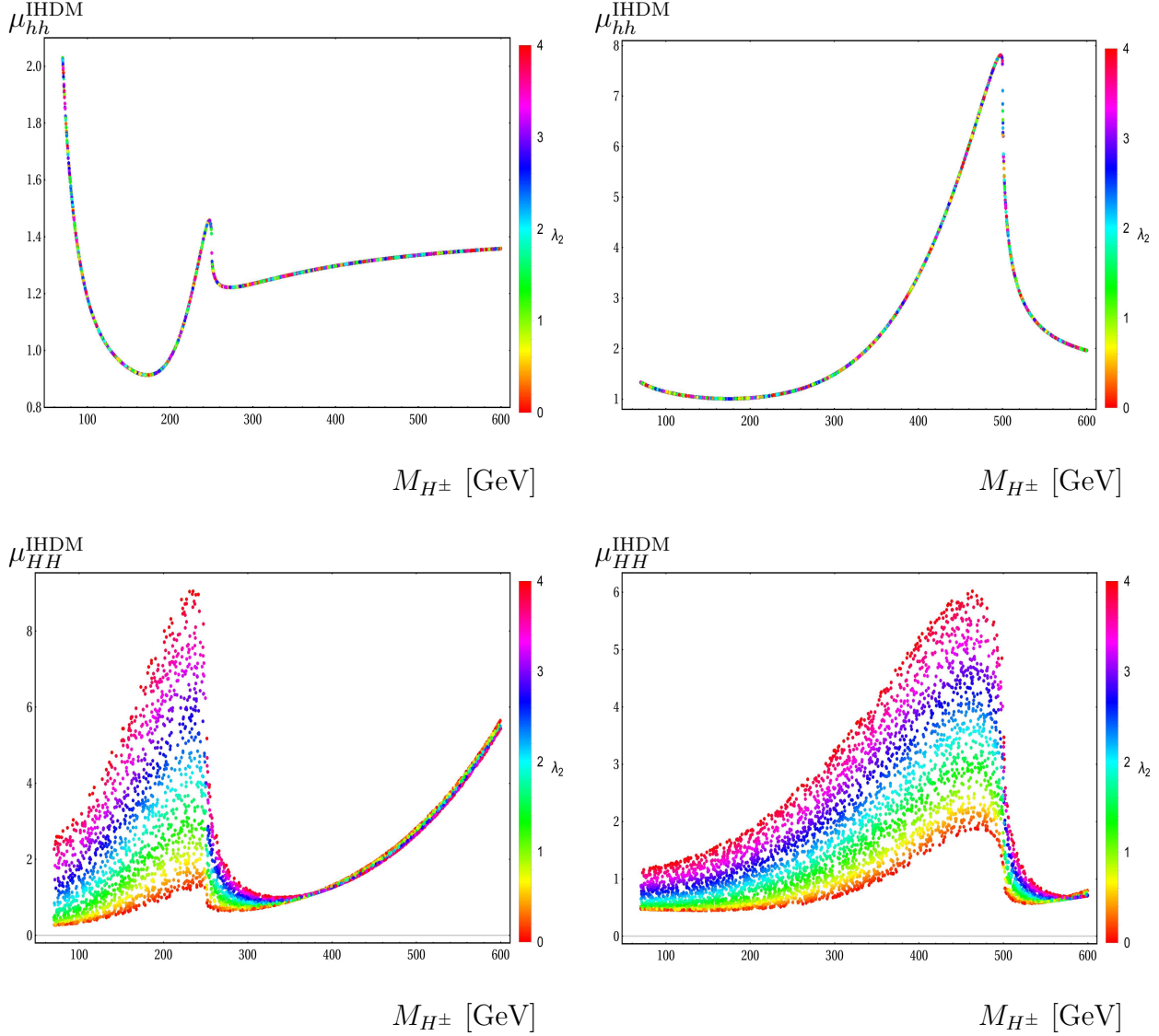


Figure 3: The enhancement factors are scanned over the parameter space of M_{H^\pm}, λ_2 . Charged Higgs masses are in $70 \text{ GeV} \leq M_{H^\pm} \leq 1000 \text{ GeV}$ and $0 \leq \lambda_2 \leq 4$. We fix $\mu_2^2 = 200^2 \text{ GeV}^2$ and $M_H = 150 \text{ GeV}$ for all cases. In the plots, we set $\sqrt{\hat{s}_{\gamma\gamma}} = 500 \text{ GeV}$ (for the above figures) and $\sqrt{\hat{s}_{\gamma\gamma}} = 1000 \text{ GeV}$ (for the below figures), correspondingly.

3.2. THDM

The phenomenological results for the production processes $\gamma\gamma \rightarrow \phi_i \phi_j$ with CP-even Higgses $\phi_{i,j} \equiv h, H$ in the THDM are analyzed in the following subsection.

3.2.1. Production cross-sections

Cross-sections for $\gamma\gamma \rightarrow \phi_i \phi_j$ in the THDM are first investigated at several CoM energies. In Fig. 4, $\hat{\sigma}_{\gamma\gamma \rightarrow \phi_i \phi_j}$ in the THDM together with $\hat{\sigma}_{\gamma\gamma \rightarrow hh}$ in the SM, are presented as functions of $\sqrt{\hat{s}_{\gamma\gamma}}$. The following data is generated at $M_{H^\pm} = 300 \text{ GeV}$, $M_H = 150 \text{ GeV}$ and $t_\beta = 5$. The CoM energies are varied as $350 \text{ GeV} \leq \sqrt{\hat{s}_{\gamma\gamma}} \leq 1500 \text{ GeV}$ in the selected-configurations. The Z_2 -breaking parameter $m_{12}^2 = M^2/s_\beta c_\beta$ is selected as follows: $M^2 = 0, 200^2, 500^2, 700^2 \text{ GeV}^2$.

In further, the mixing angle α is taken as $c_{\beta-\alpha} = +0.2$ and $s_{\beta-\alpha} = +\sqrt{1 - c_{\beta-\alpha}^2}$, accordingly. The notations for all lines appearing in the presented plots are as follows: the black line shows the cross-sections of $\gamma\gamma \rightarrow hh$ in the SM, while the blue line presents $\gamma\gamma \rightarrow hh$ in the THDM. Additionally, the green (red) line presents $\gamma\gamma \rightarrow hH$ ($\gamma\gamma \rightarrow HH$) in the THDM, respectively. Generally, we observe that $\hat{\sigma}_{\phi_i\phi_j}$ are enhanced at $\sqrt{\hat{s}_{\gamma\gamma}} \sim 2M_{H^\pm} = 600$ GeV for all cases. Among the productions, the data shows that cross-sections for $\gamma\gamma \rightarrow hH$ are suppressed compared with other productions, as a consequence of softly breaking the Z_2 -symmetry. However, $\hat{\sigma}_{hH}$ becomes more and more significant once M^2 reaches large values.

We inspect the data in the case of $M^2 = 0$. One notices that $\hat{\sigma}_{HH}$ becomes largest in the regions $\sqrt{\hat{s}_{\gamma\gamma}} \leq \sim 450$ GeV and they decrease rapidly in the regions $\sqrt{\hat{s}_{\gamma\gamma}} \geq 450$ GeV. Moreover, $\hat{\sigma}_{hh}$ in the SM and the THDM are dominant in the regions of $\sqrt{\hat{s}_{\gamma\gamma}} \geq 450$ GeV contrasted to the ones for $\gamma\gamma \rightarrow hH$, HH in the THDM. Among the mentioned cross-sections, the hh production in the THDM is largest in this case.

When $M^2 = 200^2$ GeV², the cross-sections for HH productions in THDM become largest in comparison with other ones. These massive contributions are attributed to charged Higgs in the loop. Due to the Z_2 -symmetry, the productions of hH in the THDM are still suppressed in this case. For high regions of M^2 , taking $M^2 = 500^2, 700^2$ GeV² as examples, the productions $\gamma\gamma \rightarrow hH$, HH become more and more dominant in comparison with hh production in the SM and in the THDM.

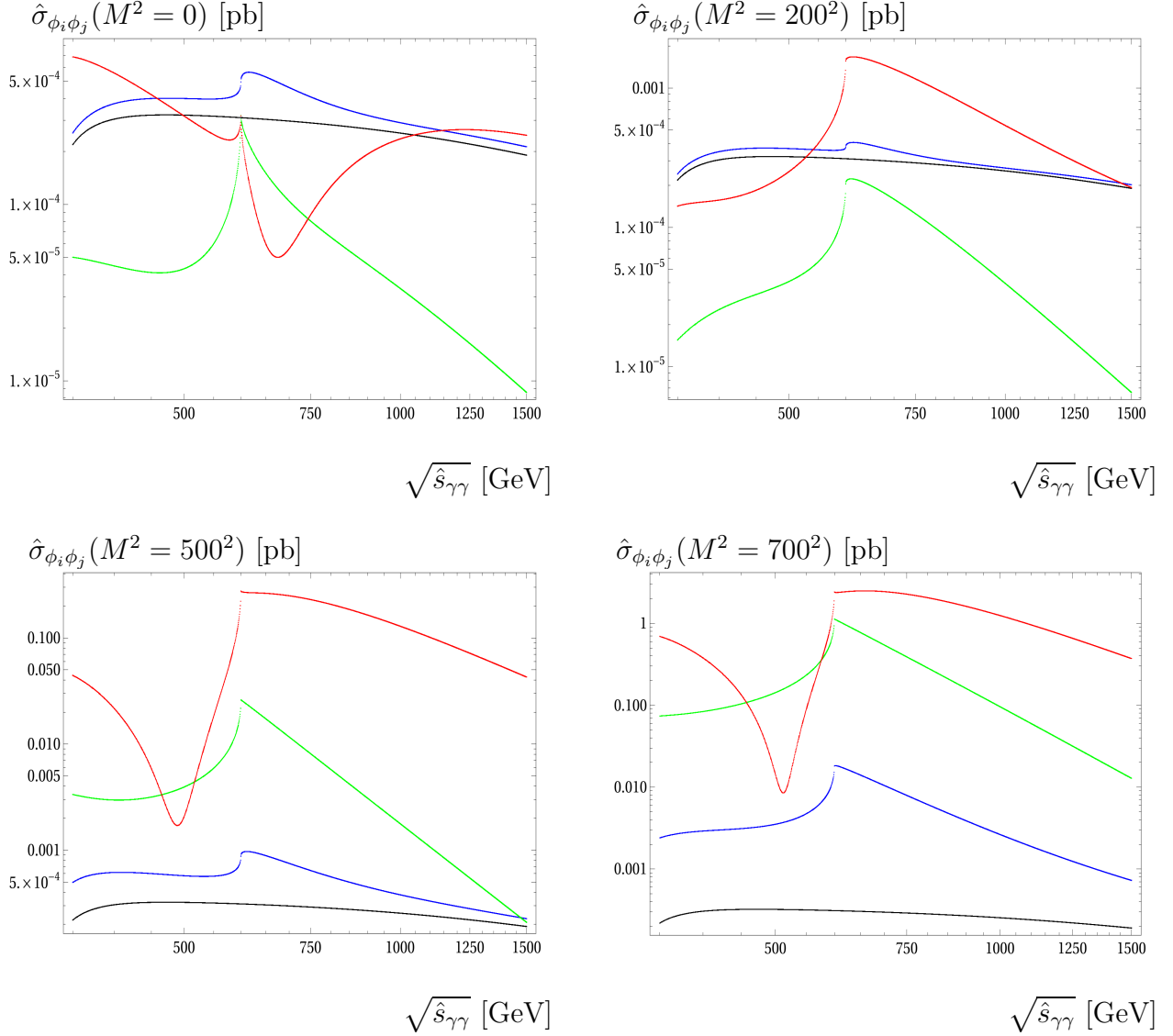


Figure 4: Cross-sections for $\gamma\gamma \rightarrow \phi_i\phi_j$ in the THDM, $\gamma\gamma \rightarrow hh$ in the SM are shown as functions of $\sqrt{\hat{s}_{\gamma\gamma}}$. In the plots, we vary $350 \text{ GeV} \leq \sqrt{\hat{s}_{\gamma\gamma}} \leq 1500 \text{ GeV}$. We select $M_{H^\pm} = 300 \text{ GeV}$, $t_\beta = 5$ in this case. Moreover, we fix $M_H = 150 \text{ GeV}$, $M^2 = 0, 200^2, 500^2, 700^2 \text{ GeV}^2$ and take $c_{\beta-\alpha} = +0.2$ and $s_{\beta-\alpha} = +\sqrt{1 - c_{\beta-\alpha}^2}$, accordingly.

3.2.2. Enhancement factors

We focus on investigating the enhancement factors defined in Eq. 24 for $\gamma\gamma \rightarrow \phi_i\phi_j$ in the THDM. The factors are first studied over the parameter space of M_{H^\pm} , t_β in this subsection. Two scenarios for $c_{\beta-\alpha} > 0$ and $c_{\beta-\alpha} < 0$ are examined in detail. In Figs. 5, 6, we fix $M^2 = M_H^2 = 200^2 \text{ GeV}^2$. Moreover, we vary $100 \text{ GeV} \leq M_{H^\pm} \leq 1000 \text{ GeV}$ and set $2 \leq t_\beta \leq 10$ in the following plots. The factors $\mu_{\phi_i\phi_j}^{\text{THDM}}$ are generated at $\sqrt{\hat{s}_{\gamma\gamma}} = 500 \text{ GeV}$ (for all the above scatter-plots) and examined at $\sqrt{\hat{s}_{\gamma\gamma}} = 1000 \text{ GeV}$ (for all the below scatter-plots). In the left panel, we show the enhancement factors for hh production. In the middle (right) panel, the enhancement factors for hH and (HH) production are presented, respectively.

In Fig. 5, the first scenario for $c_{\beta-\alpha} > 0$ is explored. In this scenario, we take $c_{\beta-\alpha} = +0.2$ as an example and $s_{\beta-\alpha} = +\sqrt{1 - c_{\beta-\alpha}^2}$, correspondingly. At $\sqrt{\hat{s}_{\gamma\gamma}} = 500 \text{ GeV}$, μ_{hh}^{THDM} changes

from 1 to 1.5 for the entire range of M_{H^\pm} . The values of μ_{hh}^{THDM} are enhanced around the peak at $M_{H^\pm} = \sqrt{\hat{s}_{\gamma\gamma}}/2 = 250$ GeV. Predominantly, the factors are proportional to t_β^{-1} in this case. Interestingly, we observe that the factors μ_{hH}^{THDM} change from 0 to 0.5 for the entire range of M_{H^\pm} . The suppressed values of μ_{hH}^{THDM} are expected, as explained in the previous paragraph, due to the Z_2 -symmetry. The μ_{HH}^{THDM} exhibit the same behavior as μ_{hh}^{THDM} , in that they are inversely proportional to t_β . On the other hand, the enhancement factors for HH productions in the THDM are strongly dependent on the charged Higgs mass but change slightly with t_β . In the entire range of M_{H^\pm} , the factors μ_{HH}^{THDM} range from 0.3 to 1.2.

At $\sqrt{\hat{s}_{\gamma\gamma}} = 1000$ GeV, the factors μ_{hh}^{THDM} become the largest at the peak at $M_{H^\pm} = \sqrt{\hat{s}_{\gamma\gamma}}/2 = 500$ GeV. Around the peak, μ_{hh}^{THDM} changes from 1.2 to 1.8. Beyond the peak, the factors change from 1.0 to 1.2 in the entire range of M_{H^\pm} . It is important to note that μ_{hh}^{THDM} slightly changes with t_β . For HH productions, μ_{HH}^{THDM} varies from 0.4 to 2.5 around the peak (at $M_{H^\pm} = 500$ GeV) regions. It is noted that μ_{HH}^{THDM} slightly changes with t_β . Otherwise, μ_{hH}^{THDM} is much smaller than 1 and is inversely proportional to t_β .

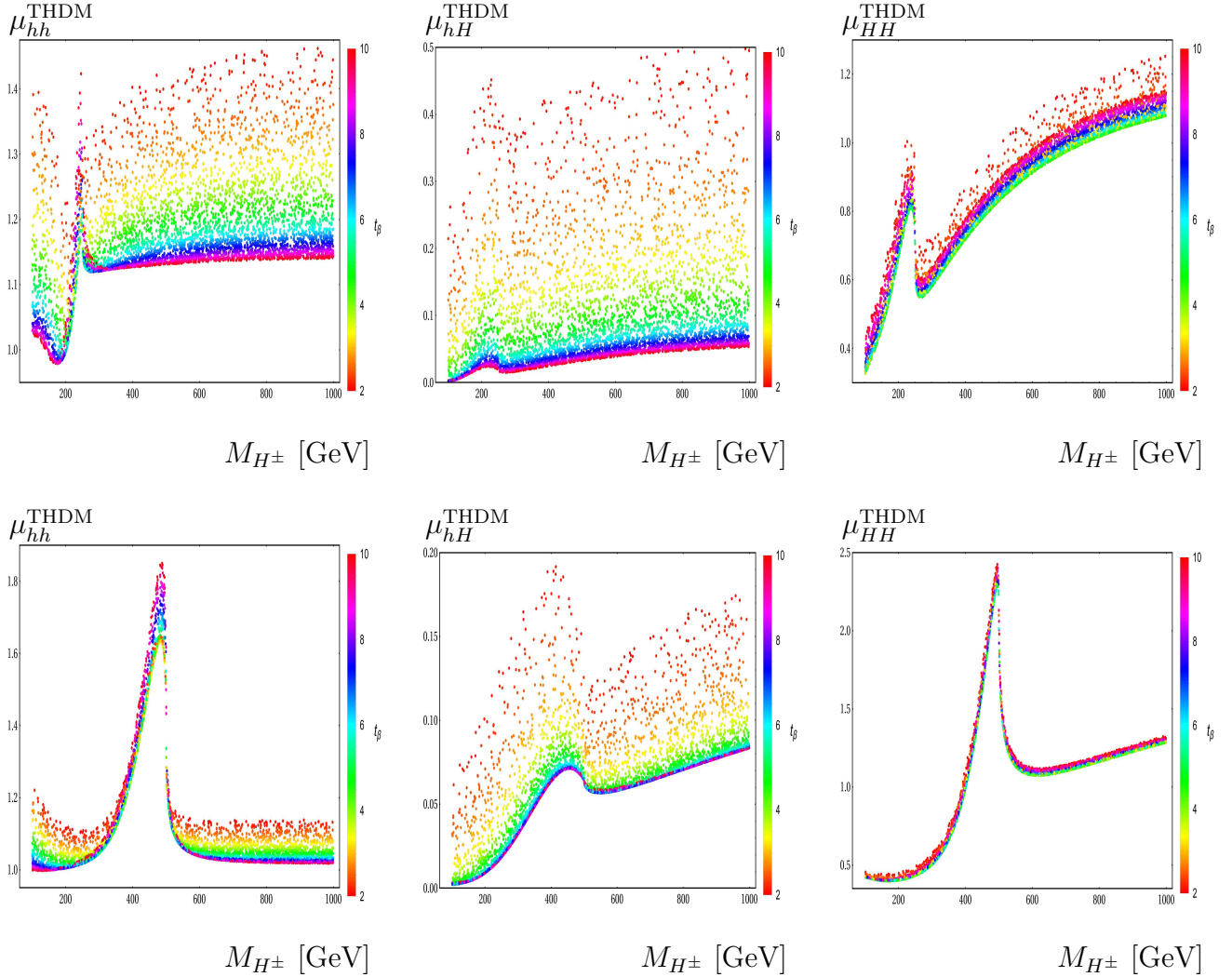


Figure 5: The enhancement factors are presented in the parameter space of M_{H^\pm} , t_β . In the plots, we fix $M^2 = M_H^2 = 200^2$ GeV² and take $c_{\beta-\alpha} = +0.2$ and $s_{\beta-\alpha} = +\sqrt{1 - c_{\beta-\alpha}^2}$, accordingly. In these plots, we set $\sqrt{\hat{s}_{\gamma\gamma}} = 500$ GeV (for the above plots) and $\sqrt{\hat{s}_{\gamma\gamma}} = 1000$ GeV (for the below plots), respectively.

Another scenario for $c_{\beta-\alpha} < 0$ is considered for examining how the factors are affected by setting a different sign of $c_{\beta-\alpha}$ in this work. In Fig. 6, we take $c_{\beta-\alpha} = -0.2$ for an example and $s_{\beta-\alpha} = +\sqrt{1 - c_{\beta-\alpha}^2}$, accordingly. At $\sqrt{\hat{s}_{\gamma\gamma}} = 500$ GeV, it is interesting to observe that μ_{hh}^{THDM} shows different behavior in comparison with the previous scenario. At this CoM energy, the factors μ_{hh}^{THDM} can reach up to 1.5 in the low region of $M_{H^\pm} < 200$ GeV. They then decrease to around 0.9 when $M_{H^\pm} > 200$ GeV. There is no peak of the factors observed in this scenario because the contributions of singly charged Higgs exchanging in the one-loop triangle diagrams may cancel out with the ones from the one-loop box diagrams in this scenario. Surprisingly, we find that the factors μ_{hh}^{THDM} are proportional to t_β in this scenario. For the hH productions, the factors are suppressed and they are in the range of $[\sim 0.025, \sim 0.3]$. They are sensitive to t_β^{-1} in all ranges of charged Higgs mass. In HH productions, it is found that the factors develop to the peak around $M_{H^\pm} = 500$ GeV. They reach a factor of 2.5 around the peak and they are in the ranges of $[\sim 0.5, \sim 1.7]$ beyond the peak regions. In all ranges of M_{H^\pm} , the factors μ_{HH}^{THDM} are proportional to t_β^{-1} in this scenario.

The survey for all the enhancement factors at $\sqrt{\hat{s}_{\gamma\gamma}} = 1000$ GeV is presented in the next paragraphs. The factors μ_{hh}^{THDM} are large in the regions ($M_{H^\pm} \leq 200$ GeV) and they can reach up to 1.5. They then decrease rapidly to the regions around $M_{H^\pm} \sim 300$ GeV and develop a peak at $M_{H^\pm} = \sqrt{\hat{s}_{\gamma\gamma}}/2 = 500$ GeV. Around the peak, the enhancement factor is about 1.2. In other ranges of charged Higgs mass, $\mu_{hh}^{\text{THDM}} \sim 0.9$. One also observes that μ_{hh}^{THDM} is inversely proportional to t_β in this scenario. In hH productions, the factors increase to the peak at $M_{H^\pm} = \sqrt{\hat{s}_{\gamma\gamma}}/2 = 500$ GeV and they are about 0.3 around the peak. In all regions of M_{H^\pm} , the mentioned factors are in the ranges of $[\sim 0.025, \sim 0.3]$ and they are inversely proportional to t_β . In the last case, it is found that the factors μ_{HH}^{THDM} show the same behavior as the previous scenario. They are in the ranges of $[\sim 0.5, \sim 4]$ in all regions of M_{H^\pm} . However, the factors μ_{HH}^{THDM} depend only slightly on t_β in this scenario.

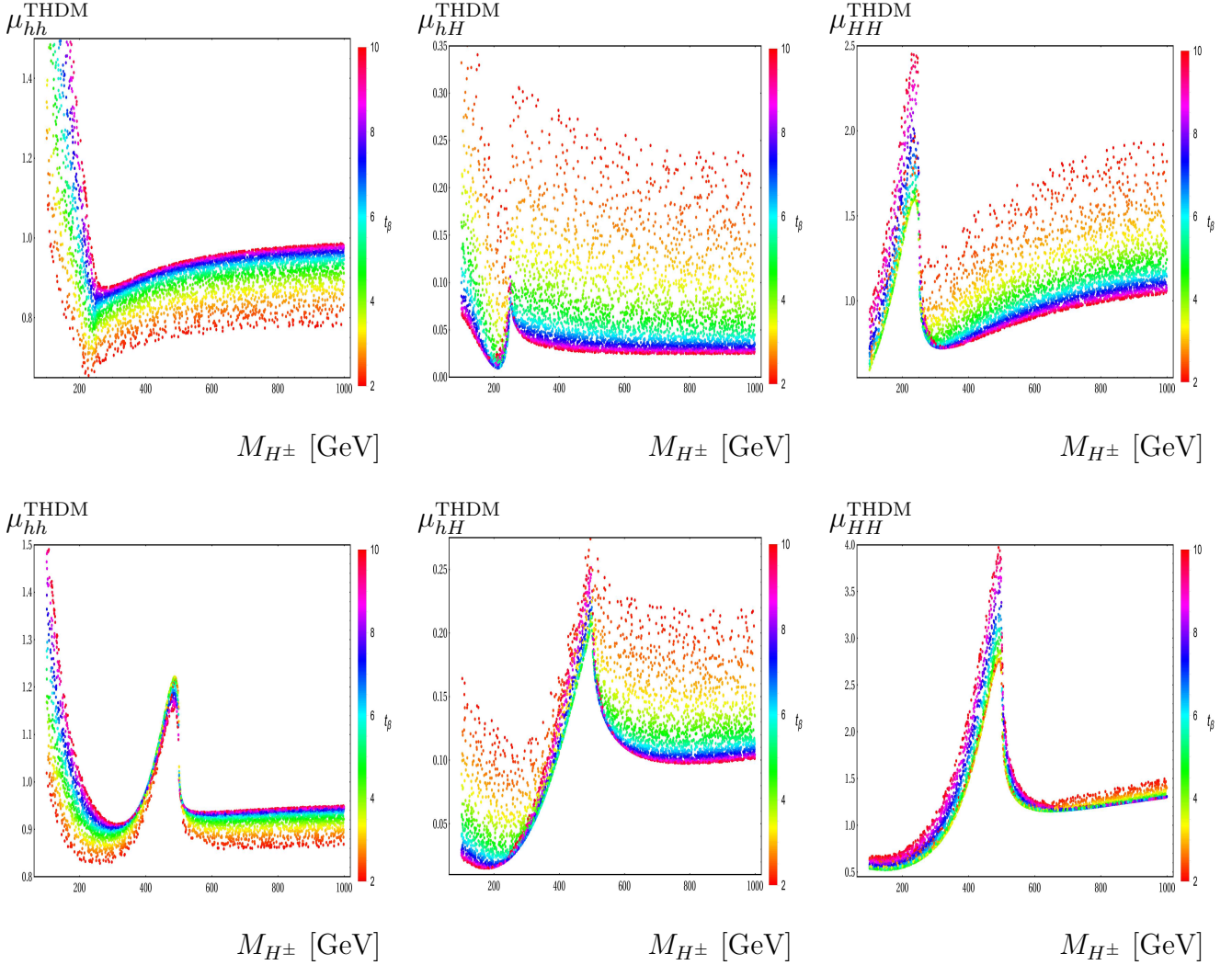


Figure 6: The enhancement factors are presented in the parameter space M_{H^\pm} , t_β . In the plots, we consider the scenario for $c_{\beta-\alpha} = -0.2 < 0$ and $s_{\beta-\alpha} = +\sqrt{1 - c_{\beta-\alpha}^2}$, correspondingly. We also fix $M^2 = M_H^2 = 200^2$ GeV² and set $\sqrt{\hat{s}_{\gamma\gamma}} = 500$ (for all the above-plots) GeV and $\sqrt{\hat{s}_{\gamma\gamma}} = 1000$ GeV (for all the below-plots).

The enhancement factors scanned over the parameter space of M_{H^\pm} , M^2 in the THDM are also of great interest in this work. Two scenarios for $c_{\beta-\alpha} > 0$ and $c_{\beta-\alpha} < 0$ are studied in detail in the following paragraphs. In Fig. 7 (for the $c_{\beta-\alpha} > 0$ scenario) and Fig. 8 (for the $c_{\beta-\alpha} < 0$ scenario), we consider $\sqrt{\hat{s}_{\gamma\gamma}} = 500$ GeV (for all the above scatter plots) and $\sqrt{\hat{s}_{\gamma\gamma}} = 1000$ GeV (for all the below scatter plots). Moreover, we vary the charged Higgs mass as $100 \text{ GeV} \leq M_{H^\pm} \leq 1000 \text{ GeV}$, the soft-breaking parameter as $0 \text{ GeV}^2 \leq M^2 \leq 200^2 \text{ GeV}^2$, and take $t_\beta = 5$ for all cases.

In Fig. 7, the first scenario of $c_{\beta-\alpha} > 0$ is examined. For this case, we take $c_{\beta-\alpha} = +0.2$ as an example and $s_{\beta-\alpha} = +\sqrt{1 - c_{\beta-\alpha}^2}$, accordingly. For hh production at $\sqrt{\hat{s}_{\gamma\gamma}} = 500$ GeV, we observe the peak of μ_{hh}^{THDM} at $M_{H^\pm} = 250$ GeV, which is corresponding to the threshold of cross-sections for hh in the THDM at the peak $\sqrt{\hat{s}_{\gamma\gamma}} = 2M_{H^\pm}$. Around the peak, μ_{hh}^{THDM} varies from 1.0 to 1.8. Above the peak regions, the enhancement factors tend to 1.2 and depend slightly on M^2 . For hH production, μ_{hH}^{THDM} is more sensitive to M^2 below the peak regions. The factors are in the range of $[0.07, 1.5]$ above the peak regions. Around the peak, μ_{hH}^{THDM} can reach up to 0.3. We also find the same behavior for μ_{HH}^{THDM} . The factors for HH production are large in the

low regions of M_{H^\pm} and around the peak $M_{H^\pm} = 250$ GeV. They are in the range of $[0.7, 2.4]$ above the peak regions. Generally, we observe that $\mu_{\phi_i\phi_j}^{\text{THDM}}$ is proportional to $1/M$ at this CoM energy.

At $\sqrt{\hat{s}_{\gamma\gamma}} = 1000$ GeV, we also find that μ_{hh}^{THDM} develops to the peak at $M_{H^\pm} = 500$ GeV, where the factors can reach up to 2.2 and decrease rapidly beyond the peak. The factors depend slightly on M^2 and tend to 1 beyond the peak regions. For hH production, μ_{hH}^{THDM} is sensitive to M^2 in the peak regions. They tend to 0.05 and are slightly dependent on M^2 in the regions above the peak. For HH production, the factors become large in the regions below the peak and they are inversely proportional to M^{-1} . Around the peak, the factors are enhanced by large values of M^2 . Above the peak regions, μ_{HH}^{THDM} varies around 1.0.

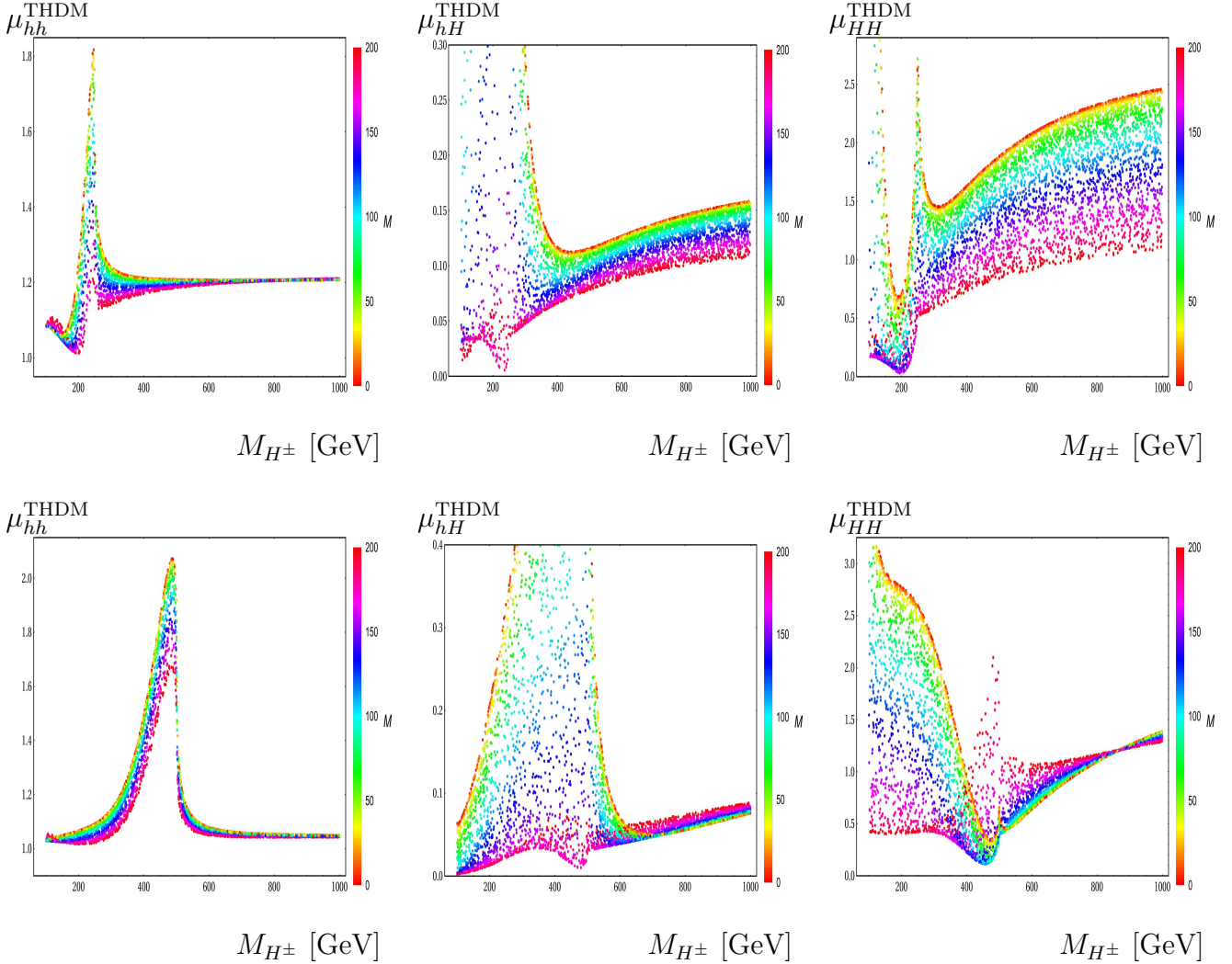


Figure 7: The enhancement factors are presented in the parameter space of M_{H^\pm} , M^2 . In the plots, we take $t_\beta = 5$ and consider the first scenario of $c_{\beta-\alpha} = +0.2$ and $s_{\beta-\alpha} = +\sqrt{1 - c_{\beta-\alpha}^2}$, accordingly. In these plots, we set $\sqrt{\hat{s}_{\gamma\gamma}} = 500$ GeV (for the above Figures) and $\sqrt{\hat{s}_{\gamma\gamma}} = 1000$ GeV (for the below Figures).

Another scenario for $c_{\beta-\alpha} = -0.2 < 0$ is also considered interestingly in this work. In Fig. 8, $s_{\beta-\alpha} = +\sqrt{1 - c_{\beta-\alpha}^2}$ is obtained accordingly. We are going to comment on the physical results at $\sqrt{\hat{s}_{\gamma\gamma}} = 500$ GeV. For hh production, we observe different behavior of μ_{hh}^{THDM} in comparison

with the $c_{\beta-\alpha} > 0$ scenario. Specifically, the factors are large in the regions below the peak. Around the peak regions, they are enhanced by the small value of M and can reach up to 1.6. Above the peak regions, the factors are in the ranges of $[0.9, 1.1]$. We also observe the different behavior for the factors in hH production compared with the previous scenario. The factors μ_{hH}^{THDM} reach large values in the below and around the peak regions and they are proportional to M . The factors μ_{hH}^{THDM} are in the ranges of $[0.2, 0.6]$ for M_{H^\pm} in the above the peak regions. In the case of HH production, μ_{HH}^{THDM} develops to the peak at $M_{H^\pm} \sim 250$ GeV. They are in the range of $[1.0, 2.4]$ in the above the peak regions. In general, the factors μ_{HH}^{THDM} depend slightly on charged Higgs mass and are proportional to $1/M$ in the above the peak regions.

We next comment on the physical results at $\sqrt{\hat{s}_{\gamma\gamma}} = 1000$ GeV. The factors μ_{hh}^{THDM} are enhanced by the small values of M in the low regions of charged Higgs mass and they can reach up to 1.2. They tend to 2.5 around the peak. The factors are then varied around ~ 0.9 . In general, the factors depend on M^{-1} . In the hH production, μ_{hH}^{THDM} is more sensitive to M^{-1} around the peak regions. They then tend to 0.2 in the high mass regions of singly charged Higgs. For HH production, the factors μ_{HH}^{THDM} strongly depend on M^{-1} . At the peak, the factors are enhanced by the large value of M . Above the peak regions, μ_{HH}^{THDM} tend to ~ 1 .

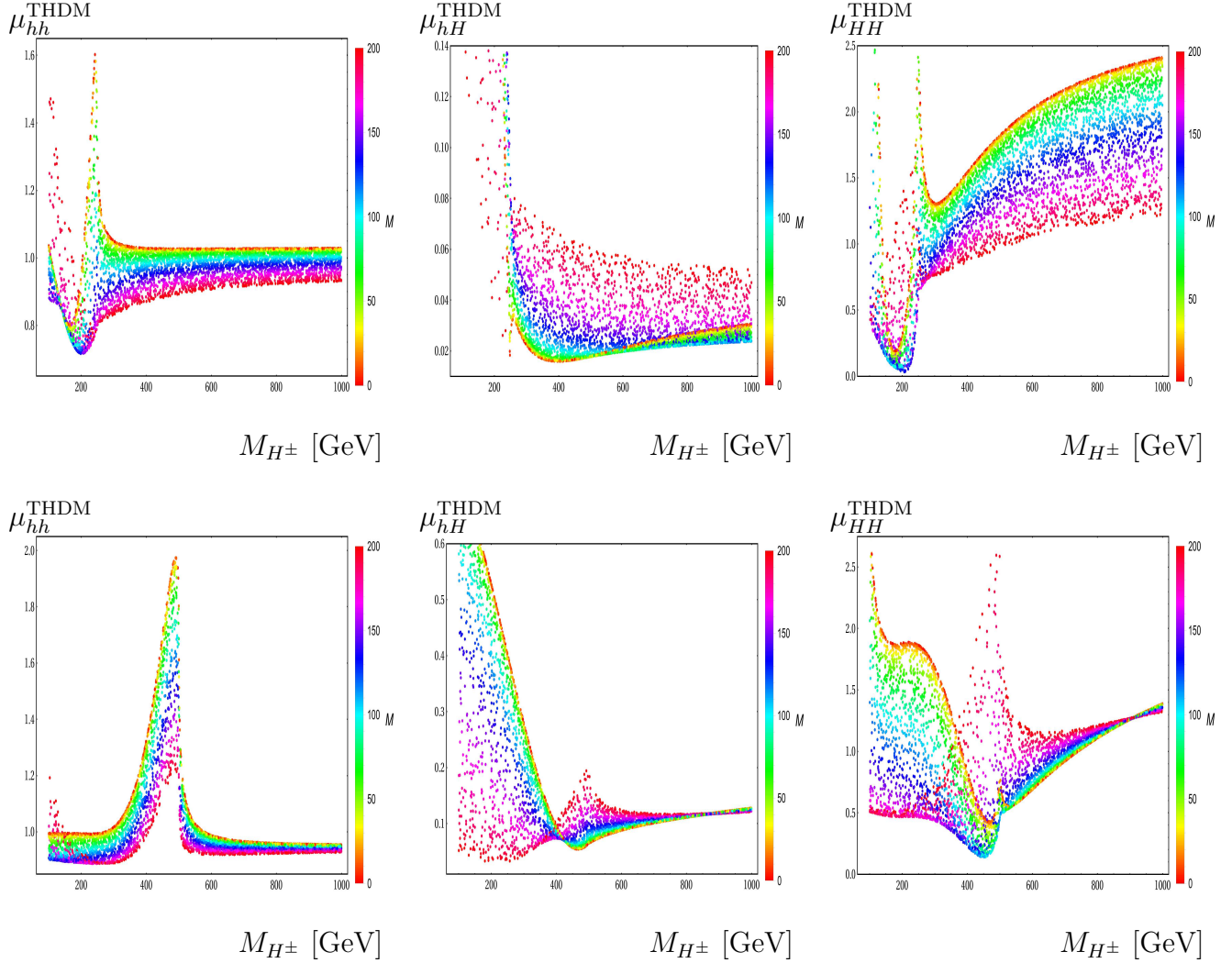


Figure 8: The enhancement factors are presented in the parameter space of M_{H^\pm} , M^2 . In the plots, we take $t_\beta = 5$ and $c_{\beta-\alpha} = -0.2$ and $s_{\beta-\alpha} = +\sqrt{1 - c_{\beta-\alpha}^2}$, accordingly. In these plots, we set $\sqrt{\hat{s}_{\gamma\gamma}} = 500$ GeV (the above Figures) and $\sqrt{\hat{s}_{\gamma\gamma}} = 1000$ GeV (the below Figures).

4. Conclusions

In this paper, we have presented the phenomenological results for one-loop induced processes $\gamma\gamma \rightarrow \phi_i\phi_j$ with CP-even Higgses $\phi_{i,j} \equiv h, H$ at high-energy photon-photon collisions in the IHDM and the THDM. In the phenomenological results, we have shown the cross sections at several center-of-mass energies. The results show that cross sections for the computed processes in the models under investigation are enhanced around the threshold of charged Higgs pair production ($\sim 2M_{H^\pm}$). Furthermore, the enhancement factors for the processes are examined in the parameter space of the models under consideration. In the IHDM, the factors are studied in the parameter space of (M_{H^\pm}, μ_2^2) and (M_{H^\pm}, λ_2) . In the THDM, the factors are analyzed in the planes of (M_{H^\pm}, t_β) and (M_{H^\pm}, M^2) . Two scenarios of $c_{\beta-\alpha} > 0$ and $c_{\beta-\alpha} < 0$ have been studied in further detail. The factors give a different behavior when considering these scenarios. As a result, discriminations for the above-mentioned scenarios can be performed at future colliders. The dependence of the cross section for the process $\gamma\gamma \rightarrow hH$ on m_{12}^2 provides a potential probe of the soft Z_2 -breaking scale in the Two Higgs Doublet Model.

Acknowledgment: This research is funded by Vietnam National Foundation for Science and Technology Development (NAFOSTED) under the grant number 103.01-2023.16.

Appendix A: Effective Lagrangian in the IHDM

The kinematic terms of Lagrangian in the IHDM can be expanded as follows:

$$\begin{aligned}
\mathcal{L}_K^{\text{IHDM}} \supset & \frac{2M_W^2}{v} W_\mu^\pm W^{\mp,\mu} h + \frac{M_Z^2}{v} h Z_\mu Z^\mu + i \frac{M_Z c_{2W}}{v} Z^\mu (H^\mp \partial_\mu H^\pm - H^\pm \partial_\mu H^\mp) \\
& + i \frac{M_Z s_{2W}}{v} A^\mu (H^\mp \partial_\mu H^\pm - H^\pm \partial_\mu H^\mp) + i \frac{2M_Z^2 c_W^2 s_W}{v} A^\mu W_\mu^\pm G^\pm \\
& + i \frac{M_W}{v} (H W^{\mp,\mu} \partial_\mu H^\pm - H^\pm W^{\mp,\mu} \partial_\mu H - H W_\mu^\pm \partial^\mu H^\mp + H^\mp W_\mu^\pm \partial^\mu H) \\
& + \frac{M_Z^2 s_{2W}^2}{v^2} A_\mu A^\mu H^\pm H^\mp + \frac{2M_Z^2 c_W^2 s_W}{v^2} H H^\pm W_\mu^\mp A^\mu + \frac{2M_W^2}{v^2} W_\mu^\pm W^{\mp,\mu} h h \\
& + \frac{2M_W^2}{v^2} W_\mu^\pm W^{\mp,\mu} H H + \frac{M_Z^2 s_{2W}^2}{v^2} A_\mu A^\mu G^\pm G^\mp \\
& + i \frac{M_Z s_{2W}}{v} A^\mu (G^\mp \partial_\mu G^\pm - G^\pm \partial_\mu G^\mp) + \dots
\end{aligned} \tag{25}$$

We also expand the scalar Higgs potential of the IHDM and collect the terms involving to Higgs self-coupling as follows:

$$\begin{aligned}
-\mathcal{V}_{\text{IHDM}}(\phi_1, \phi_2) \supset & -\frac{3M_h^2}{v} h h h + \frac{2(\mu_2^2 - M_H^2)}{v} h H H + \frac{2(\mu_2^2 - M_{H^\pm}^2)}{v} h H^\pm H^\mp \\
& + \frac{M_{H^\pm}^2 - M_H^2}{v} H H^\pm G^\mp + \frac{2(\mu_2^2 - M_{H^\pm}^2)}{v^2} h h H^\pm H^\mp - 2\lambda_2 H H H^\pm H^\mp \\
& - \frac{M_h^2}{v^2} h h G^\pm G^\mp + \frac{2(\mu_2^2 - M_{H^\pm}^2)}{v^2} H H G^\pm G^\mp + \dots
\end{aligned} \tag{26}$$

Appendix B: Effective Lagrangian in the THDM

We expand the kinematic terms of Lagrangian in the THDM as follows:

$$\begin{aligned}
\mathcal{L}_K^{\text{THDM}} \supset & \frac{2M_W^2}{v} s_{\beta-\alpha} h W_\mu^\pm W^{\mp,\mu} + \frac{2M_W^2}{v} c_{\alpha-\beta} H W_\mu^\pm W^{\mp,\mu} + \frac{M_Z^2}{v} s_{\beta-\alpha} h Z_\mu Z^\mu \\
& + \frac{M_Z^2}{v} c_{\alpha-\beta} H Z_\mu Z^\mu + i \frac{M_Z c_{2W}}{v} Z^\mu (H^\mp \partial_\mu H^\pm - H^\pm \partial_\mu H^\mp) \\
& + i \frac{M_Z s_{2W}}{v} A^\mu (H^\mp \partial_\mu H^\pm - H^\pm \partial_\mu H^\mp) + \frac{4M_W^2 s_W^2}{v^2} H^\pm H^\mp A_\mu A^\mu \\
& - i \frac{M_W s_{\beta-\alpha}}{v} (H W^{\mp,\mu} \partial_\mu H^\pm - H W^{\pm,\mu} \partial_\mu H^\mp + H^\mp W^{\pm,\mu} \partial_\mu H - H^\pm W^{\mp,\mu} \partial_\mu H) \\
& - i \frac{M_W c_{\beta-\alpha}}{v} (-h W^{\mp,\mu} \partial_\mu H^\pm + h W^{\pm,\mu} \partial_\mu H^\mp - H^\mp W^{\pm,\mu} \partial_\mu h + H^\pm W^{\mp,\mu} \partial_\mu h) \\
& + \frac{2M_W^2 s_W c_{\beta-\alpha}}{v^2} h H^\mp W_\mu^\pm A^\mu - \frac{2M_W^2 s_W s_{\beta-\alpha}}{v^2} H H^\mp W_\mu^\pm A^\mu \\
& + \frac{2M_W^2}{v^2} W_\mu^\pm W^{\mp,\mu} H H + \frac{2M_W^2}{v^2} W_\mu^\pm W^{\mp,\mu} h h + \dots
\end{aligned} \tag{27}$$

Expanding the scalar potential in the THDM, we then collect the terms involving to the Higgs self-couplings as

$$-\mathcal{V}_{\text{THDM}}(\phi_1, \phi_2) \supset -\lambda_{hHH} h H H - \lambda_{Hhh} H h h - \lambda_{hH^\pm H^\mp} h H^\pm H^\mp$$

$$-\lambda_{hH^\pm H^\mp} H H^\pm H^\mp - \lambda_{HhH^\pm H^\mp} H h H^\pm H^\mp + \dots \quad (28)$$

All coefficients of the mentioned couplings are shown explicitly in terms of physical parameters as follows:

$$-\lambda_{hHH} = \frac{3\lambda_1 v}{2} s_\alpha c_\alpha^2 c_\beta - \frac{3\lambda_2 v}{2} s_\beta s_\alpha^2 c_\alpha - \frac{\lambda_{345}}{2} v [c_\beta (2s_\alpha c_\alpha^2 - s_\alpha^3) + s_\beta (c_\alpha^3 - 2s_\alpha^2 c_\alpha)] \quad (29)$$

$$= \frac{s_{\alpha-\beta} [s_{2\alpha} (3M^2 - M_h^2 - 2M_H^2) + M^2 s_{2\beta}]}{v s_{2\beta}}, \quad (30)$$

$$-\lambda_{Hhh} = -\frac{3\lambda_1 v}{2} c_\beta c_\alpha s_\alpha^2 - \frac{3\lambda_2 v}{2} s_\beta c_\alpha^2 s_\alpha - \frac{\lambda_{345}}{2} v [s_\beta (s_\alpha^3 - 2c_\alpha^2 s_\alpha) - c_\beta (2c_\alpha s_\alpha^2 - c_\alpha^3)] \quad (31)$$

$$= \frac{c_{\alpha-\beta} [s_{2\alpha} (3M^2 - M_H^2 - 2m_h^2) - M^2 s_{2\beta}]}{v s_{2\beta}}, \quad (32)$$

$$-\lambda_{HH^\pm H^\mp} = -\lambda_1 v c_\beta c_\alpha s_\beta^2 - \lambda_2 v s_\beta s_\alpha c_\beta^2 - \lambda_3 v (s_\beta s_\alpha s_\beta^2 + c_\beta c_\alpha c_\beta^2) + \frac{\lambda_{45}}{2} v s_{(2\beta)} s_{\beta+\alpha} \quad (33)$$

$$= \frac{s_{\alpha+\beta} (4M^2 - 3M_H^2 - 2M_{H^\pm}^2) + (2M_{H^\pm}^2 - M_H^2) s_{\alpha-3\beta}}{2v s_{(2\beta)}}, \quad (34)$$

$$-\lambda_{hH^\pm H^\mp} = \lambda_1 v c_\beta s_\alpha s_\beta^2 - \lambda_2 v s_\beta c_\alpha c_\beta^2 - \lambda_3 v (s_\beta c_\alpha s_\beta^2 - c_\beta s_\alpha c_\beta^2) + \frac{\lambda_{45}}{2} v s_{(2\beta)} c_{(\beta+\alpha)} \quad (35)$$

$$= \frac{c_{\alpha+\beta} (4M^2 - 3M_h^2 - 2M_{H^\pm}^2) + (2M_{H^\pm}^2 - M_h^2) c_{(\alpha-3\beta)}}{2v s_{2\beta}}, \quad (36)$$

and

$$-\lambda_{HhH^\pm H^\mp} = \lambda_1 s_\beta^2 s_\alpha c_\alpha - \lambda_2 c_\beta^2 s_\alpha c_\alpha + \lambda_3 s_\alpha c_\alpha c_{2\beta} + (\lambda_4 + \lambda_5) s_\beta c_\beta c_{2\alpha} \quad (37)$$

$$= \frac{s_{2\alpha} (3c_{2\alpha} + c_{2(\alpha-2\beta)} - 4c_{2\beta})}{4v^2 s_{2\beta}^2} M_H^2 - \frac{s_{2\alpha} (3c_{2\alpha} + c_{2(\alpha-2\beta)} + 4c_{2\beta})}{4v^2 s_{2\beta}^2} M_h^2 \\ + \frac{s_{2(\alpha-\beta)}}{v^2} M_{H^\pm}^2 + \frac{(s_{2(\alpha-3\beta)} + 2s_{2(\alpha-\beta)} + 5s_{2(\alpha+\beta)})}{4v^2 s_{2\beta}^2} M^2, \quad (38)$$

$$-\lambda_{HhG^\pm G^\mp} = \lambda_1 c_\beta^2 s_\alpha c_\alpha - \lambda_2 s_\beta^2 s_\alpha c_\alpha - \lambda_3 s_\alpha c_\alpha c_{2\beta} - (\lambda_4 + \lambda_5) s_\beta c_\beta c_{2\alpha} \\ = \frac{1}{2v^2 s_{2\beta}} s_{2(\alpha-\beta)} [(M_h^2 - M_H^2) s_{2\alpha} + 2(M^2 - M_{H^\pm}^2) s_{2\beta}]. \quad (39)$$

Furthermore, we have the following couplings:

$$-\lambda_{hhh} = 3v \left[\lambda_1 s_\alpha^3 c_\beta - \lambda_2 c_\alpha^3 s_\beta + (\lambda_3 + \lambda_4 + \lambda_5) (s_\alpha c_\beta c_\alpha^2 - c_\alpha s_\beta s_\alpha^2) \right] \\ = \frac{3e}{4M_W s_W s_{2\beta}} \left[M^2 c_{\alpha-3\beta} + (M^2 - M_h^2) c_{3\alpha-\beta} + (2M^2 - 3M_h^2) c_{\alpha+\beta} \right], \quad (40)$$

$$-\lambda_{HHH} = -3v \left[\lambda_1 c_\alpha^3 c_\beta + \lambda_2 s_\alpha^3 s_\beta + (\lambda_3 + \lambda_4 + \lambda_5) (c_\alpha c_\beta s_\alpha^2 + s_\alpha s_\beta c_\alpha^2) \right] \\ = \frac{3e}{4M_W s_W s_{2\beta}} \left[M^2 s_{\alpha-3\beta} + (M_H^2 - M^2) s_{3\alpha-\beta} + (2M^2 - 3M_H^2) s_{\alpha+\beta} \right], \quad (41)$$

$$-\lambda_{HHH^\pm H^\mp} = -\lambda_1 c_\alpha^2 s_\beta^2 - \lambda_2 s_\alpha^2 c_\beta^2 - \lambda_3 (c_\alpha^2 c_\beta^2 + s_\alpha^2 s_\beta^2) + (\lambda_4 + \lambda_5) c_\alpha s_\alpha s_{2\beta}$$

$$\begin{aligned}
&= -\frac{2c_{\alpha-\beta}^2}{v^2}M_{H^\pm}^2 - \frac{s_{2\alpha}[3s_{2\alpha} + s_{2(\alpha-2\beta)} - 2s_{2\beta}]}{4v^2s_{2\beta}^2}M_h^2 \\
&\quad - \frac{[c_\alpha^4 + c_\alpha^3s_\alpha \cot^3\beta + c_\alpha s_\alpha^3 \cot\beta + s_\alpha^4 \cot^4\beta] \tan^2\beta}{v^2}M_H^2 \\
&\quad + \frac{s_\beta[4c_\alpha c_\beta s_\alpha + (1 + \cot^4\beta)s_\alpha^2 s_\beta + c_\alpha^2(1 + \cot^4\beta)s_\beta \tan^2\beta]}{v^2}M^2, \tag{42}
\end{aligned}$$

$$\begin{aligned}
-\lambda_{hhH^\pm H^\mp} &= -\lambda_1 s_\alpha^2 s_\beta^2 - \lambda_2 c_\alpha^2 c_\beta^2 - \lambda_3(s_\alpha^2 c_\beta^2 + c_\alpha^2 s_\beta^2) - (\lambda_4 + \lambda_5)c_\alpha s_\alpha s_{2\beta} \\
&= -\frac{2s_{\alpha-\beta}^2}{v^2}M_{H^\pm}^2 - \frac{s_{2\alpha}[3s_{2\alpha} + s_{2(\alpha-2\beta)} + 2s_{2\beta}]}{4v^2s_{2\beta}^2}M_H^2 \\
&\quad + \frac{(-c_\alpha^4 \cot^2\beta + c_\alpha s_\alpha^3 \cot\beta + c_\alpha^3 s_\alpha \tan\beta - s_\alpha^4 \tan^2\beta)}{v^2}M_h^2 \\
&\quad + \frac{s_\beta c_\beta[-4c_\alpha s_\alpha + (1 + \cot^4\beta)s_\alpha^2 \tan^3\beta + c_\alpha^2(\cot^3\beta + \tan\beta)]}{v^2}M^2, \tag{43}
\end{aligned}$$

$$\begin{aligned}
-\lambda_{hhG^\pm G^\mp} &= -\lambda_1 s_\alpha^2 c_\beta^2 - \lambda_2 c_\alpha^2 s_\beta^2 - \lambda_3(c_\alpha^2 c_\beta^2 + s_\alpha^2 s_\beta^2) + (\lambda_4 + \lambda_5)c_\alpha s_\alpha s_{2\beta} \\
&= \frac{2c_{\alpha-\beta}^2}{v^2}(M^2 - M_{H^\pm}^2) - \frac{c_{\alpha-\beta}^2 s_{2\alpha}}{v^2 s_{2\beta}}M_H^2 + \frac{-3s_{2\beta} + 2s_{2\alpha} + s_{4\alpha-2\beta}}{4v^2 s_{2\beta}}M_h^2, \tag{44}
\end{aligned}$$

$$\begin{aligned}
-\lambda_{HHG^\pm G^\mp} &= -\lambda_1 c_\alpha^2 c_\beta^2 - \lambda_2 s_\alpha^2 s_\beta^2 - \lambda_3(s_\alpha^2 c_\beta^2 + c_\alpha^2 s_\beta^2) - (\lambda_4 + \lambda_5)c_\alpha s_\alpha s_{2\beta} \\
&= \frac{2s_{\alpha-\beta}^2}{v^2}(M^2 - M_{H^\pm}^2) + \frac{s_{\alpha-\beta}^2 s_{2\alpha}}{v^2 s_{2\beta}}M_h^2 + \frac{-3s_{2\beta} - 2s_{2\alpha} + s_{4\alpha-2\beta}}{4v^2 s_{2\beta}}M_H^2. \tag{45}
\end{aligned}$$

Additionally, we also derive the couplings relating to Goldstone bosons as follows:

$$\begin{aligned}
\mathcal{L}_K^{\text{THDM}} &\supset \frac{2M_W^2 s_W}{v}A_\mu W^{\pm,\mu}G^\mp + \frac{4M_W^2 s_W^2}{v^2}A_\mu A^\mu G^\pm G^\mp \\
&\quad + i\frac{2M_W s_W}{v}A^\mu(G^\mp \partial_\mu G^\pm - G^\pm \partial_\mu G^\mp) + \dots \tag{46}
\end{aligned}$$

From scalar potential, we have

$$-\mathcal{V}(\phi_1, \phi_2) \supset -\lambda_{hH^\pm G^\mp} h H^\pm G^\mp - \lambda_{HH^\pm G^\mp} H H^\pm G^\mp + \dots \tag{47}$$

where the coefficients of the couplings are given by

$$-\lambda_{hH^\pm G^\mp} = \frac{ec_{\alpha-\beta}}{2M_W s_W}(M_{H^\pm}^2 - M_h^2), \tag{48}$$

$$-\lambda_{HH^\pm G^\mp} = \frac{es_{\alpha-\beta}}{2M_W s_W}(M_{H^\pm}^2 - M_H^2). \tag{49}$$

References

- [1] G. Aad *et al.* [ATLAS], Phys. Rev. D **106** (2022) no.5, 052001 doi:10.1103/PhysRevD.106.052001 [[arXiv:2112.11876](#) [hep-ex]].
- [2] G. Aad *et al.* [ATLAS], Phys. Rev. Lett. **114** (2015) no.8, 081802 doi:10.1103/PhysRevLett.114.081802 [[arXiv:1406.5053](#) [hep-ex]].

- [3] G. Aad *et al.* [ATLAS], Eur. Phys. J. C **75** (2015) no.9, 412 doi:10.1140/epjc/s10052-015-3628-x [[arXiv:1506.00285](#) [hep-ex]].
- [4] G. Aad *et al.* [ATLAS], Phys. Rev. D **92** (2015), 092004 doi:10.1103/PhysRevD.92.092004 [[arXiv:1509.04670](#) [hep-ex]].
- [5] A. M. Sirunyan *et al.* [CMS], JHEP **01** (2018), 054 doi:10.1007/JHEP01(2018)054 [[arXiv:1708.04188](#) [hep-ex]].
- [6] M. Aaboud *et al.* [ATLAS], JHEP **11** (2018), 040 doi:10.1007/JHEP11(2018)040 [[arXiv:1807.04873](#) [hep-ex]].
- [7] A. M. Sirunyan *et al.* [CMS], Phys. Lett. B **788** (2019), 7-36 doi:10.1016/j.physletb.2018.10.056 [[arXiv:1806.00408](#) [hep-ex]].
- [8] A. M. Sirunyan *et al.* [CMS], JHEP **03** (2021), 257 doi:10.1007/JHEP03(2021)257 [[arXiv:2011.12373](#) [hep-ex]].
- [9] A. Tumasyan *et al.* [CMS], Phys. Rev. Lett. **129** (2022) no.8, 081802 doi:10.1103/PhysRevLett.129.081802 [[arXiv:2202.09617](#) [hep-ex]].
- [10] G. Aad *et al.* [ATLAS], JHEP **07** (2023), 040 doi:10.1007/JHEP07(2023)040 [[arXiv:2209.10910](#) [hep-ex]].
- [11] G. Aad *et al.* [ATLAS], Phys. Rev. D **108** (2023) no.5, 052003 doi:10.1103/PhysRevD.108.052003 [[arXiv:2301.03212](#) [hep-ex]].
- [12] G. Aad *et al.* [ATLAS], [[arXiv:2406.09971](#) [hep-ex]].
- [13] U. Baur, T. Plehn and D. L. Rainwater, Phys. Rev. Lett. **89** (2002), 151801 doi:10.1103/PhysRevLett.89.151801 [[arXiv:hep-ph/0206024](#) [hep-ph]].
- [14] U. Baur, T. Plehn and D. L. Rainwater, Phys. Rev. D **67** (2003), 033003 doi:10.1103/PhysRevD.67.033003 [[arXiv:hep-ph/0211224](#) [hep-ph]].
- [15] G. Weiglein *et al.* [LHC/LC Study Group], Phys. Rept. **426** (2006), 47-358 doi:10.1016/j.physrep.2005.12.003 [[arXiv:hep-ph/0410364](#) [hep-ph]].
- [16] H. Baer *et al.* [ILC], [[arXiv:1306.6352](#) [hep-ph]].
- [17] V. Shiltsev and F. Zimmermann, Rev. Mod. Phys. **93** (2021), 015006 doi:10.1103/RevModPhys.93.015006 [[arXiv:2003.09084](#) [physics.acc-ph]].
- [18] A. Arhrib, R. Benbrik, C. H. Chen, R. Guedes and R. Santos, JHEP **08** (2009), 035 doi:10.1088/1126-6708/2009/08/035 [[arXiv:0906.0387](#) [hep-ph]].
- [19] J. Grigo, J. Hoff, K. Melnikov and M. Steinhauser, Nucl. Phys. B **875** (2013), 1-17 doi:10.1016/j.nuclphysb.2013.06.024 [[arXiv:1305.7340](#) [hep-ph]].
- [20] D. Y. Shao, C. S. Li, H. T. Li and J. Wang, JHEP **07** (2013), 169 doi:10.1007/JHEP07(2013)169 [[arXiv:1301.1245](#) [hep-ph]].
- [21] U. Ellwanger, JHEP **08** (2013), 077 doi:10.1007/JHEP08(2013)077 [[arXiv:1306.5541](#) [hep-ph]].

- [22] C. Han, X. Ji, L. Wu, P. Wu and J. M. Yang, JHEP **04** (2014), 003 doi:10.1007/JHEP04(2014)003 [[arXiv:1307.3790](#) [hep-ph]].
- [23] A. J. Barr, M. J. Dolan, C. Englert and M. Spannowsky, Phys. Lett. B **728** (2014), 308-313 doi:10.1016/j.physletb.2013.12.011 [[arXiv:1309.6318](#) [hep-ph]].
- [24] D. de Florian and J. Mazzitelli, Phys. Rev. Lett. **111** (2013), 201801 doi:10.1103/PhysRevLett.111.201801 [[arXiv:1309.6594](#) [hep-ph]].
- [25] N. Haba, K. Kaneta, Y. Mimura and E. Tsedenbaljir, Phys. Rev. D **89** (2014) no.1, 015018 doi:10.1103/PhysRevD.89.015018 [[arXiv:1311.0067](#) [hep-ph]].
- [26] J. Cao, D. Li, L. Shang, P. Wu and Y. Zhang, JHEP **12** (2014), 026 doi:10.1007/JHEP12(2014)026 [[arXiv:1409.8431](#) [hep-ph]].
- [27] T. Enkhbat, JHEP **01** (2014), 158 doi:10.1007/JHEP01(2014)158 [[arXiv:1311.4445](#) [hep-ph]].
- [28] Q. Li, Q. S. Yan and X. Zhao, Phys. Rev. D **89** (2014) no.3, 033015 doi:10.1103/PhysRevD.89.033015 [[arXiv:1312.3830](#) [hep-ph]].
- [29] R. Frederix, S. Frixione, V. Hirschi, F. Maltoni, O. Mattelaer, P. Torrielli, E. Vryonidou and M. Zaro, Phys. Lett. B **732** (2014), 142-149 doi:10.1016/j.physletb.2014.03.026 [[arXiv:1401.7340](#) [hep-ph]].
- [30] J. Baglio, O. Eberhardt, U. Nierste and M. Wiebusch, Phys. Rev. D **90** (2014) no.1, 015008 doi:10.1103/PhysRevD.90.015008 [[arXiv:1403.1264](#) [hep-ph]].
- [31] D. E. Ferreira de Lima, A. Papaefstathiou and M. Spannowsky, JHEP **08** (2014), 030 doi:10.1007/JHEP08(2014)030 [[arXiv:1404.7139](#) [hep-ph]].
- [32] B. Hespel, D. Lopez-Val and E. Vryonidou, JHEP **09** (2014), 124 doi:10.1007/JHEP09(2014)124 [[arXiv:1407.0281](#) [hep-ph]].
- [33] V. Barger, L. L. Everett, C. B. Jackson, A. D. Peterson and G. Shaughnessy, Phys. Rev. Lett. **114** (2015) no.1, 011801 doi:10.1103/PhysRevLett.114.011801 [[arXiv:1408.0003](#) [hep-ph]].
- [34] J. Grigo, K. Melnikov and M. Steinhauser, Nucl. Phys. B **888** (2014), 17-29 doi:10.1016/j.nuclphysb.2014.09.003 [[arXiv:1408.2422](#) [hep-ph]].
- [35] F. Maltoni, E. Vryonidou and M. Zaro, JHEP **11** (2014), 079 doi:10.1007/JHEP11(2014)079 [[arXiv:1408.6542](#) [hep-ph]].
- [36] F. Goertz, A. Papaefstathiou, L. L. Yang and J. Zurita, JHEP **04** (2015), 167 doi:10.1007/JHEP04(2015)167 [[arXiv:1410.3471](#) [hep-ph]].
- [37] A. Azatov, R. Contino, G. Panico and M. Son, Phys. Rev. D **92** (2015) no.3, 035001 doi:10.1103/PhysRevD.92.035001 [[arXiv:1502.00539](#) [hep-ph]].
- [38] A. Papaefstathiou, Phys. Rev. D **91** (2015) no.11, 113016 doi:10.1103/PhysRevD.91.113016 [[arXiv:1504.04621](#) [hep-ph]].

- [39] R. Grober, M. Muhlleitner, M. Spira and J. Streicher, JHEP **09** (2015), 092 doi:10.1007/JHEP09(2015)092 [[arXiv:1504.06577](#) [hep-ph]].
- [40] D. de Florian and J. Mazzitelli, JHEP **09** (2015), 053 doi:10.1007/JHEP09(2015)053 [[arXiv:1505.07122](#) [hep-ph]].
- [41] H. J. He, J. Ren and W. Yao, Phys. Rev. D **93** (2016) no.1, 015003 doi:10.1103/PhysRevD.93.015003 [[arXiv:1506.03302](#) [hep-ph]].
- [42] J. Grigo, J. Hoff and M. Steinhauser, Nucl. Phys. B **900** (2015), 412-430 doi:10.1016/j.nuclphysb.2015.09.012 [[arXiv:1508.00909](#) [hep-ph]].
- [43] W. J. Zhang, W. G. Ma, R. Y. Zhang, X. Z. Li, L. Guo and C. Chen, Phys. Rev. D **92** (2015), 116005 doi:10.1103/PhysRevD.92.116005 [[arXiv:1512.01766](#) [hep-ph]].
- [44] A. Agostini, G. Degrassi, R. Gröber and P. Slavich, JHEP **04** (2016), 106 doi:10.1007/JHEP04(2016)106 [[arXiv:1601.03671](#) [hep-ph]].
- [45] R. Grober, M. Muhlleitner and M. Spira, JHEP **06** (2016), 080 doi:10.1007/JHEP06(2016)080 [[arXiv:1602.05851](#) [hep-ph]].
- [46] G. Degrassi, P. P. Giardino and R. Gröber, Eur. Phys. J. C **76** (2016) no.7, 411 doi:10.1140/epjc/s10052-016-4256-9 [[arXiv:1603.00385](#) [hep-ph]].
- [47] S. Kanemura, K. Kaneta, N. Machida, S. Odori and T. Shindou, Phys. Rev. D **94** (2016) no.1, 015028 doi:10.1103/PhysRevD.94.015028 [[arXiv:1603.05588](#) [hep-ph]].
- [48] D. de Florian, M. Grazzini, C. Hanga, S. Kallweit, J. M. Lindert, P. Maierhöfer, J. Mazzitelli and D. Rathlev, JHEP **09** (2016), 151 doi:10.1007/JHEP09(2016)151 [[arXiv:1606.09519](#) [hep-ph]].
- [49] S. Borowka, N. Greiner, G. Heinrich, S. P. Jones, M. Kerner, J. Schlenk and T. Zirke, JHEP **10** (2016), 107 doi:10.1007/JHEP10(2016)107 [[arXiv:1608.04798](#) [hep-ph]].
- [50] F. Bishara, R. Contino and J. Rojo, Eur. Phys. J. C **77** (2017) no.7, 481 doi:10.1140/epjc/s10052-017-5037-9 [[arXiv:1611.03860](#) [hep-ph]].
- [51] Q. H. Cao, G. Li, B. Yan, D. M. Zhang and H. Zhang, Phys. Rev. D **96** (2017) no.9, 095031 doi:10.1103/PhysRevD.96.095031 [[arXiv:1611.09336](#) [hep-ph]].
- [52] K. Nakamura, K. Nishiwaki, K. y. Oda, S. C. Park and Y. Yamamoto, Eur. Phys. J. C **77** (2017) no.5, 273 doi:10.1140/epjc/s10052-017-4835-4 [[arXiv:1701.06137](#) [hep-ph]].
- [53] R. Grober, M. Muhlleitner and M. Spira, Nucl. Phys. B **925** (2017), 1-27 doi:10.1016/j.nuclphysb.2017.10.002 [[arXiv:1705.05314](#) [hep-ph]].
- [54] G. Heinrich, S. P. Jones, M. Kerner, G. Luisoni and E. Vryonidou, JHEP **08** (2017), 088 doi:10.1007/JHEP08(2017)088 [[arXiv:1703.09252](#) [hep-ph]].
- [55] S. Jones and S. Kuttimalai, JHEP **02** (2018), 176 doi:10.1007/JHEP02(2018)176 [[arXiv:1711.03319](#) [hep-ph]].
- [56] J. Davies, G. Mishima, M. Steinhauser and D. Wellmann, JHEP **03** (2018), 048 doi:10.1007/JHEP03(2018)048 [[arXiv:1801.09696](#) [hep-ph]].

- [57] D. Gonçalves, T. Han, F. Kling, T. Plehn and M. Takeuchi, Phys. Rev. D **97** (2018) no.11, 113004 doi:10.1103/PhysRevD.97.113004 [[arXiv:1802.04319](#) [hep-ph]].
- [58] J. Chang, K. Cheung, J. S. Lee, C. T. Lu and J. Park, Phys. Rev. D **100** (2019) no.9, 096001 doi:10.1103/PhysRevD.100.096001 [[arXiv:1804.07130](#) [hep-ph]].
- [59] G. Buchalla, M. Capozzi, A. Celis, G. Heinrich and L. Scyboz, JHEP **09** (2018), 057 doi:10.1007/JHEP09(2018)057 [[arXiv:1806.05162](#) [hep-ph]].
- [60] R. Bonciani, G. Degrassi, P. P. Giardino and R. Gröber, Phys. Rev. Lett. **121** (2018) no.16, 162003 doi:10.1103/PhysRevLett.121.162003 [[arXiv:1806.11564](#) [hep-ph]].
- [61] P. Banerjee, S. Borowka, P. K. Dhani, T. Gehrmann and V. Ravindran, JHEP **11** (2018), 130 doi:10.1007/JHEP11(2018)130 [[arXiv:1809.05388](#) [hep-ph]].
- [62] A. A H, P. Banerjee, A. Chakraborty, P. K. Dhani, P. Mukherjee, N. Rana and V. Ravindran, JHEP **05** (2019), 030 doi:10.1007/JHEP05(2019)030 [[arXiv:1811.01853](#) [hep-ph]].
- [63] J. Baglio, F. Campanario, S. Glaus, M. Mühlleitner, M. Spira and J. Streicher, Eur. Phys. J. C **79** (2019) no.6, 459 doi:10.1140/epjc/s10052-019-6973-3 [[arXiv:1811.05692](#) [hep-ph]].
- [64] J. Davies, F. Herren, G. Mishima and M. Steinhauser, JHEP **05** (2019), 157 doi:10.1007/JHEP05(2019)157 [[arXiv:1904.11998](#) [hep-ph]].
- [65] J. Davies, G. Heinrich, S. P. Jones, M. Kerner, G. Mishima, M. Steinhauser and D. Wellmann, JHEP **11** (2019), 024 doi:10.1007/JHEP11(2019)024 [[arXiv:1907.06408](#) [hep-ph]].
- [66] L. B. Chen, H. T. Li, H. S. Shao and J. Wang, Phys. Lett. B **803** (2020), 135292 doi:10.1016/j.physletb.2020.135292 [[arXiv:1909.06808](#) [hep-ph]].
- [67] L. B. Chen, H. T. Li, H. S. Shao and J. Wang, JHEP **03** (2020), 072 doi:10.1007/JHEP03(2020)072 [[arXiv:1912.13001](#) [hep-ph]].
- [68] J. Baglio, F. Campanario, S. Glaus, M. Mühlleitner, J. Ronca, M. Spira and J. Streicher, JHEP **04** (2020), 181 doi:10.1007/JHEP04(2020)181 [[arXiv:2003.03227](#) [hep-ph]].
- [69] G. Wang, Y. Wang, X. Xu, Y. Xu and L. L. Yang, Phys. Rev. D **104** (2021) no.5, L051901 doi:10.1103/PhysRevD.104.L051901 [[arXiv:2010.15649](#) [hep-ph]].
- [70] H. Abouabid, A. Arhrib, D. Azevedo, J. E. Falaki, P. M. Ferreira, M. Mühlleitner and R. Santos, JHEP **09** (2022), 011 doi:10.1007/JHEP09(2022)011 [[arXiv:2112.12515](#) [hep-ph]].
- [71] J. Davies, G. Mishima, K. Schönwald, M. Steinhauser and H. Zhang, JHEP **08** (2022), 259 doi:10.1007/JHEP08(2022)259 [[arXiv:2207.02587](#) [hep-ph]].
- [72] D. He, T. F. Feng, J. L. Yang, G. Z. Ning, H. B. Zhang and X. X. Dong, J. Phys. G **49** (2022) no.8, 085002 doi:10.1088/1361-6471/ac77a8 [[arXiv:2206.04450](#) [hep-ph]].
- [73] A. A H and H. S. Shao, JHEP **02** (2023), 067 doi:10.1007/JHEP02(2023)067 [[arXiv:2209.03914](#) [hep-ph]].
- [74] S. Iguro, T. Kitahara, Y. Omura and H. Zhang, Phys. Rev. D **107** (2023) no.7, 075017 doi:10.1103/PhysRevD.107.075017 [[arXiv:2211.00011](#) [hep-ph]].

- [75] S. Alioli, G. Billis, A. Broggio, A. Gavardi, S. Kallweit, M. A. Lim, G. Marinelli, R. Nagar and D. Napoletano, JHEP **06** (2023), 205 doi:10.1007/JHEP06(2023)205 [[arXiv:2212.10489](#) [hep-ph]].
- [76] J. Davies, K. Schönwald, M. Steinhauser and H. Zhang, JHEP **10** (2023), 033 doi:10.1007/JHEP10(2023)033 [[arXiv:2308.01355](#) [hep-ph]].
- [77] E. Bagnaschi, G. Degrossi and R. Gröber, Eur. Phys. J. C **83** (2023) no.11, 1054 doi:10.1140/epjc/s10052-023-12238-8 [[arXiv:2309.10525](#) [hep-ph]].
- [78] J. Davies, K. Schönwald, M. Steinhauser and M. Vitti, [[arXiv:2405.20372](#) [hep-ph]].
- [79] V. Brigljevic, D. Ferencek, G. Landsberg, T. Robens, M. Stamenkovic, T. Susa, H. Abouabid, A. Arhrib, H. Arnold and D. Azevedo, *et al.* [[arXiv:2407.03015](#) [hep-ph]].
- [80] G. V. Jikia, Nucl. Phys. B **412** (1994), 57-78 doi:10.1016/0550-3213(94)90494-4.
- [81] L. Z. Sun and Y. Y. Liu, Phys. Rev. D **54** (1996), 3563-3569 doi:10.1103/PhysRevD.54.3563.
- [82] S. H. Zhu, C. S. Li and C. S. Gao, Phys. Rev. D **58** (1998), 015006 doi:10.1103/PhysRevD.58.015006 [[arXiv:hep-ph/9710424](#) [hep-ph]].
- [83] S. H. Zhu, J. Phys. G **24** (1998), 1703-1721 doi:10.1088/0954-3899/24/9/005.
- [84] G. J. Gounaris and P. I. Porfyriadis, Eur. Phys. J. C **18** (2000), 181-193 doi:10.1007/s100520000520 [[arXiv:hep-ph/0007110](#) [hep-ph]].
- [85] Y. J. Zhou, W. G. Ma, H. S. Hou, R. Y. Zhang, P. J. Zhou and Y. B. Sun, Phys. Rev. D **68** (2003), 093004 doi:10.1103/PhysRevD.68.093004 [[arXiv:hep-ph/0308226](#) [hep-ph]].
- [86] F. Cornet and W. Hollik, Phys. Lett. B **669** (2008), 58-61 doi:10.1016/j.physletb.2008.09.035 [[arXiv:0808.0719](#) [hep-ph]].
- [87] E. Asakawa, D. Harada, S. Kanemura, Y. Okada and K. Tsumura, Phys. Lett. B **672** (2009), 354-360 doi:10.1016/j.physletb.2009.01.050 [[arXiv:0809.0094](#) [hep-ph]].
- [88] E. Asakawa, D. Harada, S. Kanemura, Y. Okada and K. Tsumura, [[arXiv:0902.2458](#) [hep-ph]].
- [89] T. Takahashi, N. Maeda, K. Ikematsu, K. Fujii, E. Asakawa, D. Harada, S. Kanemura, Y. Kurihara and Y. Okada, [[arXiv:0902.3377](#) [hep-ex]].
- [90] R. N. Hodgkinson, D. Lopez-Val and J. Sola, Phys. Lett. B **673** (2009), 47-56 doi:10.1016/j.physletb.2009.02.009 [[arXiv:0901.2257](#) [hep-ph]].
- [91] A. Arhrib, R. Benbrik, C. H. Chen and R. Santos, Phys. Rev. D **80** (2009), 015010 doi:10.1103/PhysRevD.80.015010 [[arXiv:0901.3380](#) [hep-ph]].
- [92] E. Asakawa, D. Harada, S. Kanemura, Y. Okada and K. Tsumura, Phys. Rev. D **82** (2010), 115002 doi:10.1103/PhysRevD.82.115002 [[arXiv:1009.4670](#) [hep-ph]].
- [93] J. Hernandez-Sanchez, C. G. Honorato, M. A. Perez and J. J. Toscano, Phys. Rev. D **85** (2012), 015020 doi:10.1103/PhysRevD.85.015020 [[arXiv:1108.4074](#) [hep-ph]].

- [94] W. Ma, C. X. Yue and T. T. Zhang, Chin. Phys. C **35** (2011), 333-338 doi:10.1088/1674-1137/35/4/003.
- [95] J. Sola and D. Lopez-Val, Nuovo Cim. C **34S1** (2011), 57-67 doi:10.1393/ncc/i2011-11002-1 [[arXiv:1107.1305](#) [hep-ph]].
- [96] Z. Heng, L. Shang and P. Wan, JHEP **10** (2013), 047 doi:10.1007/JHEP10(2013)047 [[arXiv:1306.0279](#) [hep-ph]].
- [97] M. Chiesa, B. Mele and F. Piccinini, Eur. Phys. J. C **84** (2024) no.5, 543 doi:10.1140/epjc/s10052-024-12882-8 [[arXiv:2109.10109](#) [hep-ph]].
- [98] B. Samarakoon and T. M. Figy, Phys. Rev. D **109** (2024) no.7, 075015 doi:10.1103/PhysRevD.109.075015 [[arXiv:2312.12594](#) [hep-ph]].
- [99] M. Demirci, Turk. J. Phys. **43** (2019) no.5, 442-458 doi:10.3906/fiz-1903-15 [[arXiv:1902.07236](#) [hep-ph]].
- [100] K. H. Phan, D. T. Tran and T. H. Nguyen, [[arXiv:2410.06827](#) [hep-ph]].
- [101] D. Borah and J. M. Cline, Phys. Rev. D **86** (2012), 055001 doi:10.1103/PhysRevD.86.055001 [[arXiv:1204.4722](#) [hep-ph]].
- [102] M. Gustafsson, S. Rydbeck, L. Lopez-Honorez and E. Lundstrom, Phys. Rev. D **86** (2012), 075019 doi:10.1103/PhysRevD.86.075019 [[arXiv:1206.6316](#) [hep-ph]].
- [103] A. Arhrib, R. Benbrik and N. Gaur, Phys. Rev. D **85** (2012), 095021 doi:10.1103/PhysRevD.85.095021 [[arXiv:1201.2644](#) [hep-ph]].
- [104] M. Klasen, C. E. Yaguna and J. D. Ruiz-Alvarez, Phys. Rev. D **87** (2013), 075025 doi:10.1103/PhysRevD.87.075025 [[arXiv:1302.1657](#) [hep-ph]].
- [105] M. Krawczyk, D. Sokolowska, P. Swaczyna and B. Swiezewska, JHEP **09** (2013), 055 doi:10.1007/JHEP09(2013)055 [[arXiv:1305.6266](#) [hep-ph]].
- [106] A. Arhrib, R. Benbrik and T. C. Yuan, Eur. Phys. J. C **74** (2014), 2892 doi:10.1140/epjc/s10052-014-2892-5 [[arXiv:1401.6698](#) [hep-ph]].
- [107] N. Chakrabarty, D. K. Ghosh, B. Mukhopadhyaya and I. Saha, Phys. Rev. D **92** (2015) no.1, 015002 doi:10.1103/PhysRevD.92.015002 [[arXiv:1501.03700](#) [hep-ph]].
- [108] A. Ilnicka, M. Krawczyk and T. Robens, Phys. Rev. D **93** (2016) no.5, 055026 doi:10.1103/PhysRevD.93.055026 [[arXiv:1508.01671](#) [hep-ph]].
- [109] A. Datta, N. Ganguly, N. Khan and S. Rakshit, Phys. Rev. D **95** (2017) no.1, 015017 doi:10.1103/PhysRevD.95.015017 [[arXiv:1610.00648](#) [hep-ph]].
- [110] J. Kalinowski, W. Kotlarski, T. Robens, D. Sokolowska and A. F. Zarnecki, JHEP **12** (2018), 081 doi:10.1007/JHEP12(2018)081 [[arXiv:1809.07712](#) [hep-ph]].
- [111] D. Dercks and T. Robens, Eur. Phys. J. C **79** (2019) no.11, 924 doi:10.1140/epjc/s10052-019-7436-6 [[arXiv:1812.07913](#) [hep-ph]].
- [112] C. W. Chiang and K. Yagyu, Phys. Rev. D **87** (2013) no.3, 033003 doi:10.1103/PhysRevD.87.033003 [[arXiv:1207.1065](#) [hep-ph]].

- [113] R. Benbrik, M. Boukidi, M. Ouchemhou, L. Rahili and O. Tibssirte, Nucl. Phys. B **990** (2023), 116154 doi:10.1016/j.nuclphysb.2023.116154 [[arXiv:2211.12546](#) [hep-ph]].
- [114] G. C. Branco, P. M. Ferreira, L. Lavoura, M. N. Rebelo, M. Sher and J. P. Silva, Phys. Rept. **516** (2012), 1-102 doi:10.1016/j.physrep.2012.02.002 [[arXiv:1106.0034](#) [hep-ph]].
- [115] M. Aoki, S. Kanemura, K. Tsumura and K. Yagyu, Phys. Rev. D **80** (2009), 015017 doi:10.1103/PhysRevD.80.015017 [[arXiv:0902.4665](#) [hep-ph]].
- [116] S. Nie and M. Sher, Phys. Lett. B **449** (1999), 89-92 doi:10.1016/S0370-2693(99)00019-2 [[arXiv:hep-ph/9811234](#) [hep-ph]].
- [117] S. Kanemura, T. Kasai and Y. Okada, Phys. Lett. B **471** (1999), 182-190 doi:10.1016/S0370-2693(99)01351-9 [[arXiv:hep-ph/9903289](#) [hep-ph]].
- [118] A. G. Akeroyd, A. Arhrib and E. M. Naimi, Phys. Lett. B **490** (2000), 119-124 doi:10.1016/S0370-2693(00)00962-X [[arXiv:hep-ph/0006035](#) [hep-ph]].
- [119] I. F. Ginzburg and I. P. Ivanov, Phys. Rev. D **72** (2005), 115010 doi:10.1103/PhysRevD.72.115010 [[arXiv:hep-ph/0508020](#) [hep-ph]].
- [120] S. Kanemura, Y. Okada, H. Taniguchi and K. Tsumura, Phys. Lett. B **704** (2011), 303-307 doi:10.1016/j.physletb.2011.09.035 [[arXiv:1108.3297](#) [hep-ph]].
- [121] S. Kanemura and K. Yagyu, Phys. Lett. B **751** (2015), 289-296 doi:10.1016/j.physletb.2015.10.047 [[arXiv:1509.06060](#) [hep-ph]].
- [122] L. Bian and N. Chen, JHEP **09** (2016), 069 doi:10.1007/JHEP09(2016)069 [[arXiv:1607.02703](#) [hep-ph]].
- [123] W. Xie, R. Benbrik, A. Habjia, S. Taj, B. Gong and Q. S. Yan, Phys. Rev. D **103** (2021) no.9, 095030 doi:10.1103/PhysRevD.103.095030 [[arXiv:1812.02597](#) [hep-ph]].
- [124] J. Haller, A. Hoecker, R. Kogler, K. Mönig, T. Peiffer and J. Stelzer, Eur. Phys. J. C **78** (2018) no.8, 675 doi:10.1140/epjc/s10052-018-6131-3 [[arXiv:1803.01853](#) [hep-ph]].
- [125] K. H. Phan, D. T. Tran and T. H. Nguyen, PTEP **2024** (2024) no.8, 083B02 doi:10.1093/ptep/ptae103 [[arXiv:2404.02417](#) [hep-ph]].
- [126] K. H. Phan, D. T. Tran and T. H. Nguyen, [[arXiv:2406.15749](#) [hep-ph]].